



HAL
open science

Characteristics of the low-level jets observed over Dunkerque (North Sea French coast) using 4 years of wind lidar data

Elsa Dieudonné, Hervé Delbarre, Anton Sokolov, Felix Ebojie, Patrick Augustin, Marc Fourmentin

► **To cite this version:**

Elsa Dieudonné, Hervé Delbarre, Anton Sokolov, Felix Ebojie, Patrick Augustin, et al.. Characteristics of the low-level jets observed over Dunkerque (North Sea French coast) using 4 years of wind lidar data. *Quarterly Journal of the Royal Meteorological Society*, 2023, 149 (754), pp.1745-1768. 10.1002/qj.4480 . hal-04291006

HAL Id: hal-04291006

<https://ulco.hal.science/hal-04291006>

Submitted on 22 Nov 2023

HAL is a multi-disciplinary open access archive for the deposit and dissemination of scientific research documents, whether they are published or not. The documents may come from teaching and research institutions in France or abroad, or from public or private research centers.

L'archive ouverte pluridisciplinaire **HAL**, est destinée au dépôt et à la diffusion de documents scientifiques de niveau recherche, publiés ou non, émanant des établissements d'enseignement et de recherche français ou étrangers, des laboratoires publics ou privés.

RESEARCH ARTICLE

Characteristics of the low-level jets observed over Dunkerque (North Sea French coast) using 4 years of wind lidar data

Elsa Dieudonné¹ | Hervé Delbarre¹ | Anton Sokolov¹ | Felix Ebojie |
Patrick Augustin¹ | Marc Fourmentin¹

Laboratoire de Physico-Chimie de l'Atmosphère (LPCA), Université du Littoral Côte d'Opale (ULCO) Dunkerque, Dunkirk, France

Correspondence

Elsa Dieudonné, Laboratoire de Physico-Chimie de l'Atmosphère (LPCA), Université du Littoral Côte d'Opale (ULCO), Dunkerque, France.

Email: elsa.dieudonne@univ-littoral.fr

Funding information

Agence Nationale de la Recherche Labex CaPPA, ANR-11-LABX-0005-01; Conseil Régional Hauts-de-France CPER Climibio, Labex CaPPA; European Regional Development Fund; Ministère de l'Éducation Nationale, de l'Enseignement Supérieur et de la Recherche CPER Climibio

Abstract

This study investigates the occurrence and characteristics of low-level jets (LLJs) up to 200 m above sea level in the North Sea area, specifically in the southernmost part of the basin, at the entrance of the English Channel. Using a short-range Doppler lidar installed in Dunkerque Port, on the northern coast of France, wind profiles were recorded for 4 years and analyzed statistically. LLJs were detected on more than 11,000 of the 10-min average wind profiles (5% of time), with similar jet core height and core speed distributions as in other sites in the southern North Sea area, and a similar annual cycle. However, there were differences in the core directions and the daily cycle, with afternoon northeasterly jets being the most frequent in Dunkerque, whereas southwesterly nocturnal jets were dominant in the other North Sea sites. This suggests that wind channeling in the Dover Strait is likely a major factor for LLJ formation in Dunkerque region. The study also examined the conditions of LLJ occurrence using European Centre for Medium-Range Weather Forecast (ECMWF) reanalysis v5 and ultrasonic anemometer data, but the different types of LLJs sharing the same core direction and occurrence conditions made it difficult to quantify specific jet formation mechanisms. This is the first experimental study on the North Sea shore, and at the entrance of the English Channel, providing valuable insights into the LLJ behavior in the region.

KEYWORDS

low-level jet, North Sea, wind lidar

This is an open access article under the terms of the [Creative Commons Attribution-NonCommercial](https://creativecommons.org/licenses/by-nc/4.0/) License, which permits use, distribution and reproduction in any medium, provided the original work is properly cited and is not used for commercial purposes.

© 2023 The Authors. *Quarterly Journal of the Royal Meteorological Society* published by John Wiley & Sons Ltd on behalf of Royal Meteorological Society.

1 | INTRODUCTION

Low-level jets (LLJs) are thin narrow streams of fast-moving air in the lower troposphere. They were first reported in the late 1930s over Africa (Gouault, 1938; Farquharson, 1939) and were later observed over every other continent (e.g., Means, 1952; Smedman *et al.*, 1993; Andreas *et al.*, 2000; Du *et al.*, 2012). LLJs typically occur between 80 and 1,500 m above ground level (AGL) and have been found to appear at altitudes as low as 30 m above the sea surface in stably stratified boundary layers (Smedman *et al.*, 1993; Smedman *et al.*, 1995). LLJs are an important atmospheric process, as their frequency of occurrence in the Earth's boundary layer is far from negligible (e.g., Blackadar, 1957; Bonner, 1968). Their study has drawn considerable attention owing to their impact on weather, regional climate, pollution transport and dispersion, aviation safety, and wind energy production.

Numerous studies have demonstrated the role of LLJs in the transport of heat and moisture from the ocean to the deep inland, along with their role in the initiation of shear instabilities for storm development (e.g., from the Gulf of Mexico to the US Great Plains; McCorcle, 1988; Wu and Raman, 1998). Therefore, LLJs play a role in deep convection, precipitation, and in the development of severe weather phenomena, such as mesoscale convective complexes, squall lines, and tornadoes (e.g., Means, 1944; Maddox, 1983; Frisch *et al.*, 1992; Zhong *et al.*, 1996). For instance, a LLJ was heavily involved in the US Great Plains flooding of 1993 and drought event of 1988 (e.g., Schwerdtfeger, 1975; Mo *et al.*, 1995; Arritt *et al.*, 1997). In addition to moisture, LLJs have been linked to the transport of air pollutants, before mixing them down to the surface, degrading the air quality up to several tens of kilometers away from the source regions (e.g., for ozone Corsmeier, 1997; Banta *et al.*, 1998; Klein *et al.*, 2019). The transport by LLJs also concerns the smoke from wildland or forest fires (Sharples, 2009) and greenhouse gases, which affects the estimation of their emissions using boundary-layer budget techniques (Mathieu *et al.*, 2005; Karipot *et al.*, 2006).

From a more local point of view, the strong vertical wind shear created by LLJs generates mechanical turbulence aloft that can be transported down to the ground (Mahrt, 1999; Banta *et al.*, 2002) and tends to increase the vertical mixing below the jet (Banta *et al.*, 2006; Karipot *et al.*, 2006). The wind shear associated with LLJs also affects aviation safety, as abrupt changes in the headwind result in just as abrupt changes in the air lift, and thus aircraft height, which may cause severe difficulties for landing or take-off, particularly for small aircraft (FAA Safety Team, 2008; Golding, 2005). The occurrence of LLJs is also an important parameter to consider during the site selection and design process of a wind farm, as LLJs

have a profound impact on wind energy production (e.g., Christakos *et al.*, 2014; Gutierrez *et al.*, 2014; Nunalee and Basu, 2014). The wind speed increases substantially inside a jet, which can improve the capacity factor of the turbine (ratio of the average power generated to the rated peak power); however, the LLJ vertical wind shear creates a vertical gradient in the thrust forces exerted by the wind on the blades, which increases the fatigue of the turbine (Gutierrez *et al.*, 2014). The short-term prediction of the generated electric power is also complicated by the presence of a strong wind shear, which poses problems in integrating the wind farm into the electric grid.

In the North Sea region, previous LLJ studies were based on anemometer and Doppler lidar data from offshore platforms located about 40–90 km from the Dutch or German coast (Kettle, 2014; Kalverla *et al.*, 2017; Duncan, 2018; Wagner *et al.*, 2019a; Møller *et al.*, 2020) or from inland sites located about 40–50 km from the Dutch coast (Baas *et al.*, 2009) or from the German coast (Wildmann *et al.*, 2022), or even farther inland in northern Germany (Ziemann *et al.*, 2020; Weide Luiz and Fiedler, 2022). This work aims at completing the knowledge of LLJs in the North Sea area by documenting their characteristics in a coastal area and at a site located at the southern edge of the North Sea, close to the entrance of the English Channel. Compared with previous studies, such a coastal environment is expected to favor baroclinic effects associated with land–sea temperature gradients; that is, land/sea breezes. In addition to these local circulations, the vicinity of the English Channel may generate regional LLJs as the wind is channeled by the Dover Strait (Capon, 2003).

In this study, the LLJs have been characterized using 4 years of high-resolution wind profiles from a short-range Doppler lidar, completed by a sonic anemometer for near-surface winds. The observations, which allow detection of jets up to 200 m above sea level, were recorded above the port of Dunkerque (Dunkirk in English), a French city located on the southernmost part of the North Sea, about 40 km east of the English Channel exit. This study was first triggered by the announcement of the installation of an offshore wind farm close to the city (<https://parc-eolien-en-mer-de-dunkerque.fr/>), which raised questions about the wind energy availability and extreme weather phenomena in the region. However, Dunkerque city also hosts several large industrial facilities (steelworks, aluminum foundry, petro- and agro-chemistry, etc.), so that acquiring a better knowledge of the LLJs' characteristics was also important to better understand pollutant dispersion in such a coastal industrial city. In addition, LLJs can present a problem for the navigation of the largest ships in the English Channel and during port entrance and docking maneuvers (the air draft of a recent container ship can reach ~75 m).

Thus, we focus on the characteristics of LLJs and provide a detailed discussion about their frequency of occurrence, and their diurnal and seasonal variations over the region, in regard to previous observations, notably recorded in and around the North Sea. The rest of this article is organized as follows: Section 2 provides information about the study site, the observations and reanalysis data used, and the data analysis process; Section 3 presents the results (retrieved jet properties, diurnal and seasonal variability, weather conditions associated with LLJ occurrence in the Dunkerque region); Section 4 contains the discussion; and Section 5 summarizes the paper and concludes.

2 | OBSERVATIONS AND DATA PROCESSING

2.1 | Experimental set-up and data availability

The study site, Dunkerque, is located in the extreme north of France (51.05° N, 2.35° E), on the southern coast of the North Sea and close to the entrance of the English Channel (Figure 1a). The coastline in this area is generally oriented from southsouthwest to eastnortheast and is bordered by a very flat terrain, the southern Flanders Plain, that extends about 15 km inland and has a mean elevation of ~ 5 m above mean sea level (AMSL); it is limited to the southeast by low hills about 30 to 40 m AMSL.

This study mainly relies on wind profiles retrieved from a Doppler lidar (WindCube v2; Vaisala, Saclay,

France) installed in Dunkerque harbor (Figure 1b). Actually, two lidars were used: the first one was installed at the entrance of the port (red dot in Figure 1b) and recorded observation over 1 year; then, after a few months' interruption, another lidar of the same model was installed in the inner port (yellow star in Figure 1b). At both locations, the lidar was set up on the roof of a small building ~ 14 m AMSL. The lidar retrieved the three wind components using the Doppler beam swinging technique with a combination of five beams (four in the cardinal directions at a 62° elevation angle from the ground, plus a vertical beam). The accumulation time was 1 s for each beam, so that a wind profile was retrieved every 5 s, with an accuracy of $0.1 \text{ m}\cdot\text{s}^{-1}$. The wind profiles were then averaged over 10-min periods. The wind was retrieved every 20 m from 40 to 220 m above the instrument; the observation altitudes were therefore 54, 74, 94, 114, 134, 154, 174, 194, 214, and 234 m AMSL. For the second series of observations in the inner port, two higher gates were added; the exact altitudes varied in time within a maximum of 304 m AMSL (maximum range of the instrument). An automatic filter was applied to the data, and all measurements having a carrier-to-noise ratio lower than -23 dB were discarded. In the presence of clouds or during rainfall, the carrier-to-noise ratio drops with increasing altitude, so that the wind observations' availability decreases with altitude. However, the data availability is above 95.7% for all levels up to 244 m AMSL, dropping to $\sim 70\%$ at 274 m AMSL and $\sim 49\%$ at 304 m AMSL.

The lidar observation at the port entrance cover the period from July 29, 2016, to July 30, 2017, with

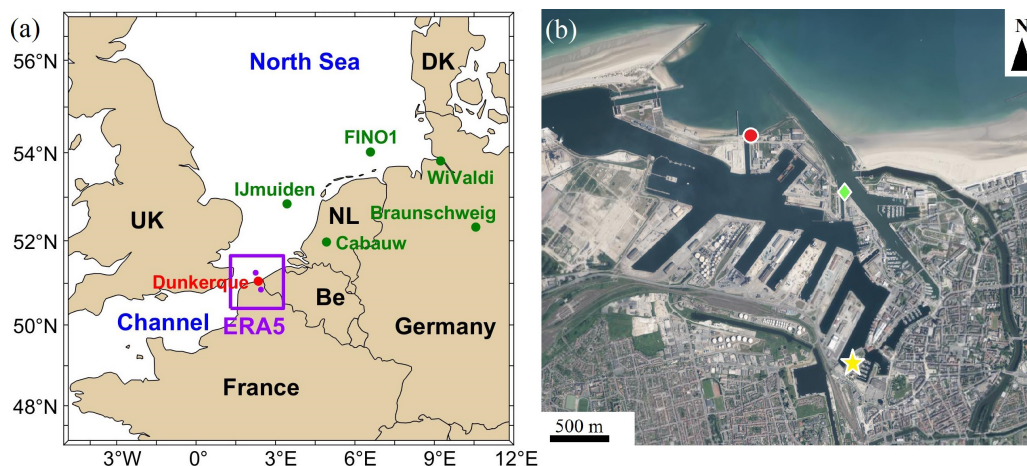


FIGURE 1 (a) Map showing the location of Dunkerque city (red dot) and the places where previous studies of low-level jets in the North Sea area took place (green dots), plus the boundaries of the domain for which ERA5 data were retrieved (purple square) with the two points used to compute the land–sea temperature gradient (purple dots). Be: Belgium; NL: Netherlands; DK: Denmark. (b) Aerial picture of Dunkerque city center and the eastern side of the harbor showing the locations of the Doppler lidar (red dot from July 2016 to July 2017, yellow star from November 2017 onwards) and of the ultrasonic anemometer (green diamond) (background image from <https://www.geoportail.gouv.fr/>) [Colour figure can be viewed at [wileyonlinelibrary.com](https://onlinelibrary.com)]

only 15 days missing in June 2017 due to power failure. The lidar observations at the inner port cover the period from November 27, 2017, to September 30, 2021, with several interruptions, as this instrument was used for other projects. Hence, a few days are missing in September 2018; there was a 4-month interruption from mid-December 2018 to mid-April 2019, a 1-month interruption in June–July 2019, and a 13-day interruption in August–September 2019. The periods with or without observations are represented graphically in Supporting Information Figure S1. In total, the database gathers 227,694 wind profiles, corresponding to 1,581 days of 10-min observations, or 4.33 years. As the lidar measurements started and ended in the middle of a calendar year, when studying the year-to-year variability, the yearly totals will be computed using reference periods ranging from the month of August to the month of July the next year.

Owing to the interruption existing in the lidar measurements, the different seasons and months of the year did not have the same number of observations (Supporting Information Table S1). The months with the lowest data availability were July (72%) and September (76%), whereas May (100%) and December (92%) had the highest data availability; all the other months of the year had a data availability between 80% and 88%. In terms of season, summer had the lowest data availability (79%), whereas spring had the highest (89%); the two other seasons had a data availability around 80–85%. In order to compute representative annual and seasonal cycles (Section 3.3), the numbers of LLJ wind profiles were corrected for these differences in data availability: the observed numbers were simply divided by the fraction of available data. This way, the figures presented in Section 3.3 correspond to the number of profiles that would have been observed if the series of measurements had been continuous, assuming that the existing observations were representative of the time period they stand for. The raw and corrected numbers underlying the figures in Section 3.3 are all given in Supporting Information Table S1.

The near-surface wind was measured using a Metek USA-1 “Scientific” three-dimension ultrasonic anemometer (Metek GmbH, Elmshorn, Germany) that was installed in the port, in between the two lidar positions (green diamond in Figure 1b), ~0.9 km from the first lidar location and ~1.4 km from the second. The mast was 15 m high, so the anemometer was located ~22 m AMSL. There are no elevated buildings in the vicinity, and the anemometer is mounted on the top of the mast, so no wind sector needs to be excluded. The ultrasonic anemometer started measuring a few months later than the lidar, on January 5, 2017, and then worked till the end of the period. The anemometer data were recorded at a 20 Hz frequency, but only the data averaged over 15 min were stored, along

with the turbulence parameters computed online from the 20 Hz data. They were later linearly interpolated to match the lidar 10-min averaging periods. It was not possible to directly average the anemometer data over 10-min periods as the raw data were not kept for storage-capacity reasons. The anemometer data were filtered using a 90% threshold on the fraction of good quality data obtained during the averaging period, which resulted in removing 0.35% of the 10-min periods (in this case, the wind profiles were kept with a missing value of the lower altitude). This did not impact the detection of LLJs, as periods with low data availability on the ultrasonic anemometer also correspond to a strongly reduced measurement range on the wind lidar (heavy rain notably). All times are given in the Universal Time Coordinate (UTC) system, which is very close to the local solar time.

2.2 | Jet detection, properties retrieval, and classification

In this work, the term LLJ refers to any stream with a low-altitude maximum in the wind profile that is at least $2 \text{ m}\cdot\text{s}^{-1}$ and 25% greater than the speed minimum located immediately above it, following the definition used in the other studies performed in the North Sea region (e.g., Baas *et al.*, 2009; Kalverla *et al.*, 2017; Wagner *et al.*, 2019b). The relative threshold of +25% is used to discard wind fluctuations unrelated to a jet event, which can go above the absolute threshold of $+2 \text{ m}\cdot\text{s}^{-1}$ during storm episodes. Other researchers (e.g., Andreas *et al.*, 2000; Karipot *et al.*, 2006) also required that the wind decreased by at least $2 \text{ m}\cdot\text{s}^{-1}$ below the maximum. However, in Dunkerque, we found that the very low altitude wind maxima often corresponded to the end or beginning of frontal passages, so we do not see any physical reason for excluding them from the jet database. Moreover, we did not have near-surface wind measurements (e.g., at a 2 m altitude) that would allow us to observe the wind decrease close to the ground (and such measurements would not be reliable in an urban area like Dunkerque). Nevertheless, the dataset was also processed adding the “wind decrease below the jet” criterion in order to assess its impact on the results (using the same absolute and relative thresholds on the wind speed). Regarding the wind absolute threshold, other studies used higher absolute values, sometimes associated with shear criteria (e.g., Bonner, 1968; Whiteman *et al.*, 1997; Song *et al.*, 2005). Aird *et al.* (2021) performed an extensive sensitivity study and showed that the number of jets detected depends greatly on the absolute and relative criteria used. In this study, we retained only the most frequently used set of speed criteria for better comparability with other studies. Also, using higher thresholds

would filter out many of the low-speed jets, which are often observed below 200 m AGL. Although those weak jets do not play a large role in the long-range transport of atmospheric species, they play a key role in the wind power estimates, turbulence generation in the surface layer, and surface–atmosphere exchanges of energy and trace gases (e.g., Mathieu *et al.*, 2005; Karipot *et al.*, 2006).

The LLJs fulfilling the aforementioned criteria were detected among the 10-min-average wind profiles from the Doppler lidar. Profiles with missing data at some altitudes were also used, provided that at least two measurements were retained above the wind maximum. In this way, jets up to 194 m AMSL could be detected during the first lidar period (1 year), and up to 234 m AMSL during the second period (3.33 years). A time continuity criterion was also used; that is, we required the wind maximum to persist during at least two consecutive 10-min profiles, so that intermittent and continuous jet events were both considered. Other researchers retained longer duration thresholds: for instance, Ziemann *et al.* (2020) used a 30-min continuity criterion (three consecutive 10-min average profiles), whereas Baas *et al.* (2009) used 1.5 hr (three consecutive 30-min average profiles). To assess the impact of the minimum duration criterion, we also processed the data imposing the jet to persist for three, six, or nine consecutive 10-min profiles.

For each of the selected wind profiles, the three following LLJ characteristics were retrieved: the jet core height, core speed, and core direction; that is, the altitude z_m , the speed V_m , and the direction θ_m of the elevated horizontal wind maximum. Height and direction continuity criteria were also tested, imposing the core altitude not to vary by more than three or two measurement heights between two consecutive profiles, and the core direction not to vary by more than 30° or 20° . The wind speed shear between the jet core and the near-surface wind was computed as the ratio $(V_m - V_s) / (z_m - z_s)$, where V_s is the wind speed from the sonic anemometer and z_s its altitude (22 m AMSL). We also computed the wind direction shear, defined as $(\theta_m - \theta_s) / (z_m - z_s)$, where θ_s is the direction of the wind from the sonic anemometer; the shear is therefore positive when the wind veers in the clockwise direction with increasing altitude. To allow comparison with other studies in the wind energy field, the shear in speed was also computed as the shear exponent α , defined as

$$\frac{V_m}{V_s} = \left(\frac{z_m}{z_s} \right)^\alpha. \quad (1)$$

To understand and explain the characteristics of the LLJs, the wind-speed cores were divided into six bins: 0th to 5th percentiles ($2 \leq V_m < 3.56 \text{ m}\cdot\text{s}^{-1}$), 5th to 25th percentiles ($3.56 \leq V_m < 5.65 \text{ m}\cdot\text{s}^{-1}$), second quartile ($5.65 \leq$

$V_m < 7.61 \text{ m}\cdot\text{s}^{-1}$), third quartile ($7.61 \leq V_m < 9.66 \text{ m}\cdot\text{s}^{-1}$), 75th to 95th percentiles ($9.66 \leq V_m < 13.33 \text{ m}\cdot\text{s}^{-1}$), 95th percentile and above ($V_m \geq 13.33 \text{ m}\cdot\text{s}^{-1}$). Additionally, in order to investigate the jet formation mechanisms, we classified the profiles based on the jet provenance. Four modes were used, following the wind rose of the jet core direction (see Section 3.2.2 and Figure 3b): northeasterly jets ($0^\circ < \theta_m \leq 80^\circ$), eastsoutheasterly jets ($80^\circ < \theta_m \leq 140^\circ$), southerly jets ($140^\circ < \theta_m \leq 230^\circ$) and westerly to northwesterly jets ($230^\circ < \theta_m \leq 360^\circ$). The coast in Dunkerque is oriented toward westsouthwest and east-northeast (azimuths 60° and 255°), so the eastsoutheasterly and southerly jet modes were offshore, whereas the northeasterly and westerly to northwesterly jet modes were onshore (Figure 3b). We also differentiated the nocturnal and diurnal wind profiles; for this, we calculated the sunrise and sunset time for each day, simply using the sunRiseSet Matlab function written by Droste (version 2.3, committed on November 6, 2017, <https://github.com/rdroste/sunRiseSet>; see also Meeus, 1991).

All the statistics presented in Section 3 (except Section 3.3.3) were computed relative to the total number of 10-min average wind profiles exhibiting a jet (herein only referred as “jet profile” or “LLJ profile”). However, it is sometimes more interesting to reason in terms of meteorological events, which requires gathering the wind profiles into continuous time-series corresponding to the same jet event. This was done using a time-continuity criterion: wind profiles with jets that were separated by less than 3 hr were considered to belong to the same event. This threshold value was set empirically by observing the time series of jet core direction along with the corresponding event attribution (e.g., Supporting Information Figure S5). A 3 hr threshold allowed us to encompass events during which the altitude of the jet core temporarily rose above 194 m AMSL, or events during which the speed increment temporarily fell below $+2 \text{ m}\cdot\text{s}^{-1}$ or $+25\%$. Very few cases were found for which this threshold resulted in mixing into the same LLJ event two different weather phenomena closely following each other in time.

2.3 | Characterizing the weather conditions

In order to characterize the weather conditions favoring the occurrence of LLJs, we used weather data from the European Centre for Medium-Range Weather Forecast (ECMWF) reanalysis v5 (ERA5; Hersbach *et al.*, 2020) available from the Copernicus Climate Change Service Climate Data Store (<https://cds.climate.copernicus.eu/>). The horizontal resolution was 0.25° , and we retrieved data on a grid surrounding Dunkerque, composed of six points

in latitude (from 50.40° N to 51.65° N) and nine points in longitude (from 1.30° E to 3.30° E). This corresponds to a quasi-square domain of 140 km × 139 km (Figure 1a). The time resolution was 1 hr, and data were linearly interpolated to match the exact time of the observed wind profiles. Two parameters were retrieved from the reanalyses: the geopotential at the 850 hPa pressure level and the 2 m temperature.

The geopotential was used to compute the geostrophic wind over Dunkerque region, using a planar fit to retrieve the orientation and strength of the geopotential gradient. The 850 hPa pressure level (~1,500 m AMSL) is commonly used as a reference as it is generally located out of the boundary layer, and thus not influenced by the surface (e.g., Blackadar, 1957; Wagner *et al.*, 2019b). The 850 hPa geostrophic wind was used to characterize the general weather conditions in the Dunkerque area, with easterly gentle flows being associated with anticyclonic conditions and stronger westerly flows corresponding to low-pressure systems passing over the region. The 2-m temperature was used to compute the land–sea temperature gradient, defined as the temperature difference between two points (Figure 1a) located over the sea northnorthwest from Dunkerque (51.25° N, 2.25° E) and over land south-southeast from Dunkerque (50.85° N, 2.45° E). Those two points are roughly symmetrical around Dunkerque on a transect from the coastline, each located ~23 km from the coastline. The temperature at each of those points was computed using bilinear interpolation from the gridded 2-m temperature. This gradient tells whether the conditions are favorable to the formation of a sea breeze on the Dunkerque coast.

Finally, the atmospheric stability was assessed using the Monin–Obukhov stability parameter Λ derived from the ultrasonic anemometer observations following

$$\Lambda = -\frac{\kappa g \overline{w'T'}}{\overline{T} u_*^3}, \quad (2)$$

where $\kappa = 0.37$ is the von-Karman constant and $g = 9.81 \text{ m}\cdot\text{s}^{-2}$ is the gravity acceleration. $\overline{w'T'}$ is the sensible heat flux and \overline{T} (K) is the average temperature, computed using the temperature measured by the anemometer, which is very close from the virtual temperature appearing in the original formula (Bardal *et al.*, 2018 and references therein). u_* is the friction velocity computed from the momentum fluxes. Other researchers use directly the Monin–Obukhov length $L = \Lambda^{-1}$ (e.g., Bardal *et al.*, 2018) or the Obukhov parameter; that is, the ratio between the measurement altitude and the Monin–Obukhov length (e.g., Rodrigo *et al.*, 2015). In this study, the Obukhov parameter was not used because the ultrasonic anemometer is installed at the very land–sea

interface so that the measurement altitude should be taken above ground level or above sea level depending on the wind direction. Values of the stability parameter were sorted into modified Pasquill stability classes (Golder, 1972; Mohan and Siddiqui, 1998); the class boundaries corresponded to a 50 cm roughness length, a value that was adjusted for the Dunkerque site during a previous study (Xiang, 2011). The atmosphere was considered to be “extremely unstable” if $\Lambda < -0.072 \text{ m}^{-1}$, “moderately unstable” if $-0.072 \leq \Lambda < -0.015 \text{ m}^{-1}$, “slightly unstable” if $-0.015 \leq \Lambda < -0.002 \text{ m}^{-1}$, “neutral” if $-0.002 \leq \Lambda < +0.003 \text{ m}^{-1}$, “moderately stable” if $0.003 \leq \Lambda < 0.016 \text{ m}^{-1}$, and “extremely stable” if $\Lambda \geq 0.016 \text{ m}^{-1}$. The months of August to December 2016 were not considered for this parameter, as the anemometer did not function at this time.

3 | RESULTS

3.1 | Sensitivity to the jet detection criteria

After processing the whole dataset, 11,462 wind profiles were found to fulfill the criteria defined in Section 2.2, which lay the basis for a robust statistical study of LLJ properties over the study site. As a preliminary remark, a total of 12,105 profiles (i.e., 5.6% more) would have been found using only the absolute detection criterion ($+2 \text{ m}\cdot\text{s}^{-1}$), so that adding the relative detection criterion ($+25\%$ wind speed) did not change the results drastically. The 11,462 selected profiles represent 5.03% of the total number of 10-min average periods with observations. This fraction depended on the year (Table 1, upper part) and varied between 3.93% (August 2017 to July 2018) and 6.41% (August 2019 to July 2020). Part of this variability might come from the data availability: when the missing periods cover preferentially the months with the highest LLJ occurrence, the fraction of time with LLJ will be underestimated. Thus, during the period with the lowest jet fraction (August 2017 to July 2018), the month of August was missing, though it is usually one of the months with the highest LLJ activity (Section 3.3.1); conversely, the period with the highest jet fraction (August 2019 to July 2020) only lacks 13 days of observations. However, the distribution of the selected wind profiles in time (Supporting Information Figure S1), clearly showed that, for the same month of the year, the number of LLJs can vary strongly from one year to the next (one can compare, for instance, the months of April 2017 or 2018 with the month of April 2020, or August 2018 with August 2019 or 2020). The fraction of time with LLJs can rise up to 22% during some months (April 2020 with 100% data availability), so that jets are definitely not

TABLE 1 Number of 10-min average wind profiles in which a low-level jet (LLJ) was detected, total number of wind profile observations, and fraction of observations with a LLJ. In the upper part, the numbers are given for 12-month periods from August to July the following year, all using the 20-min time-continuity criterion. In the lower part, the numbers are given for the whole period, varying the continuity criteria. The whole-period total does not match the sum of the yearly values as the months of August and September 2021 are not included in the yearly totals

Period	Continuity criteria	No. wind profiles	No. LLJ profiles	Fraction with LLJ (%)
August 2016–July 2017	20 min	50,250	2,008	4.00
August 2017–July 2018		36,330	1,426	3.93
August 2018–July 2019		29,120	1,309	4.50
August 2019–July 2020		50,875	3,263	6.41
August 2020–July 2021		52,124	3,043	5.84
Whole period	20 min	227,694	11,462	5.03
	30 min		8,796	3.86
	60 min		7,416	3.26
	90 min		4,993	2.19
	20 min + 30° + 3 heights		11,135	4.89
	20 min + 20° + 2 heights		10,774	4.73
	20 min + elevated jet		8,432	3.70

a negligible phenomenon for regional weather, pollutant dispersion, and wind power generation.

As could be expected, the number of LLJ wind profiles retained and the corresponding fraction of time progressively decreased as the number of consecutive profiles required was increased (Table 1, lower part). The increase from 20 to 30 min had a strong effect, as it reduced the number of profiles by 23%, whereas a further increase to 60 min only removed an extra 12% of the 20-min database. Applying the strictest criterion of 90 min, only 44% of the 20-min database remained, resulting in a fraction of time with jets of 2.19% instead of 5.03%. In the rest of the article, the looser time-continuity criterion of 20 min was used in order to include also the short-lasting jet events. Indeed, peering through the data by eye revealed that these events were not artifacts, but often seemed to be associated with frontal passages. Adding height and direction continuity criteria had a much weaker effect on the number of profiles retained than increasing the minimum duration criterion did: imposing the core altitude to vary at most by two measurement heights and the core direction at most by 20° reduced the number of selected profiles by only 6.0%. These criteria were not retained in the following, as we regularly found cases when a nocturnal LLJ would develop shortly after the end of a sea breeze, with different core properties. Finally, imposing the wind to decrease also below the jet core reduced the number of selected profiles by 26%. This criterion was not retained for the same reason as the longer time-continuity thresholds:

in order to include events associated with frontal passages, which can happen very close to the ground. The effects of stricter criteria on the results will be discussed in more detail in Section 4, but it did not change significantly the results in terms of jet properties or temporal variability.

3.2 | Jet properties

The whole LLJ database was first used altogether to derive multiannual averaged distributions of the LLJs' characteristics. Here, the fractions of LLJ wind profiles were defined as the ratio of the number of 10-min periods with specific LLJ characteristics to the total number of 10-min periods with LLJs.

3.2.1 | Jet core speed

A single value of wind retrieved in the jet core reached a speed of $33.1 \text{ m}\cdot\text{s}^{-1}$, and only four profiles (0.03% of the total) had a core speed above $18 \text{ m}\cdot\text{s}^{-1}$, so the distribution presented in Figure 2 is cropped to this value. The peak of the core speed distribution coincided with its median value ($7.6 \text{ m}\cdot\text{s}^{-1}$) and was relatively symmetric (first and third quartiles at $\sim 5.7 \text{ m}\cdot\text{s}^{-1}$ and $9.7 \text{ m}\cdot\text{s}^{-1}$ respectively). However, the core speed distribution had a longer tail on the right-hand side, so the average LLJ core speeds ($7.8 \text{ m}\cdot\text{s}^{-1}$)

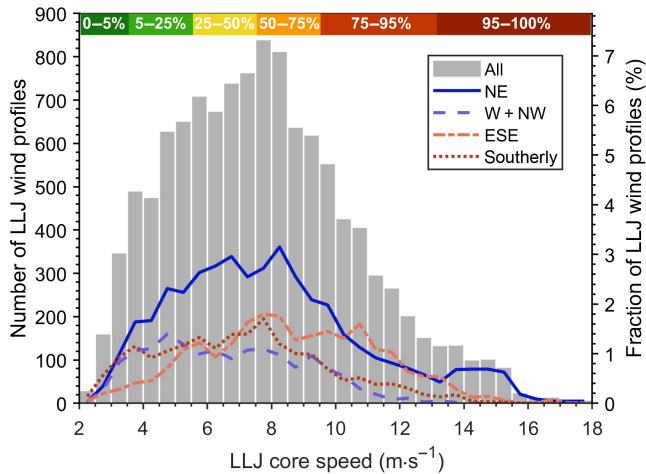


FIGURE 2 Distribution of the Low-Level Jet (LLJ) core speeds, detailed by direction mode as defined in Section 2.2. The fractions on the right y-scale are all relative to the total number of profiles with LLJ (11,462). The band on the top of the panel indicates the ranges of the six speed classes defined in Section 2.2 in terms of data percentiles. [Colour figure can be viewed at [wileyonlinelibrary.com](https://onlinelibrary.com)]

was slightly higher than the median, and the 5th and 95th percentiles ($\sim 3.6 \text{ m}\cdot\text{s}^{-1}$ and $13.3 \text{ m}\cdot\text{s}^{-1}$ respectively) were not symmetric around the median. The standard deviation was $3.0 \text{ m}\cdot\text{s}^{-1}$.

The detail of the core speed distribution in terms of direction mode (Sections 2.2 and 3.2.2) is also presented in Figure 2. The northeasterly and southerly modes had a speed distribution similar to the global distribution; the westerly + northwesterly mode had a flat distribution limited to weak and moderate core winds (below $10 \text{ m}\cdot\text{s}^{-1}$);

the eastsoutheasterly mode also had a flat distribution with a plateau extending to stronger core wind values ($5\text{--}13 \text{ m}\cdot\text{s}^{-1}$). Consequently, the strong jets belonged dominantly to the northeasterly and eastsoutheasterly modes. The strongest jets (above $14 \text{ m}\cdot\text{s}^{-1}$) were almost all northeasterly, even producing a small secondary peak in the northeasterly mode core-speed distribution (from 13.5 to $15.5 \text{ m}\cdot\text{s}^{-1}$), which is also visible from the jet core wind rose (Figure 3b).

3.2.2 | Jet core direction

The general distribution of the wind directions in Dunkerque is presented in Figure 3a, using observations recorded 100 m above the lidar; that is, 114 m AMSL as reference. All wind directions were represented, though southwesterly winds were more frequent and gathered a higher number of strong wind events, as expected due to the influence of Atlantic low-pressure systems in the region. The distribution of the LLJs' core directions (Figure 3b) was quite different from the general wind distribution, as it was dominated by onshore coastwise flows entering the English Channel and coming from the north to north-northeast directions. This "northeasterly mode", gathering wind origins from 0° to 80° , accounted for 42% of the total LLJ profiles and gathered most of the strong jet profiles (as already stated in Section 3.2.1). The orography in the Dover Strait region is not so elevated, but in association with the sea-land surface roughness gradient, it has been shown to be able to channel the wind and generate LLJs (Capon, 2003).

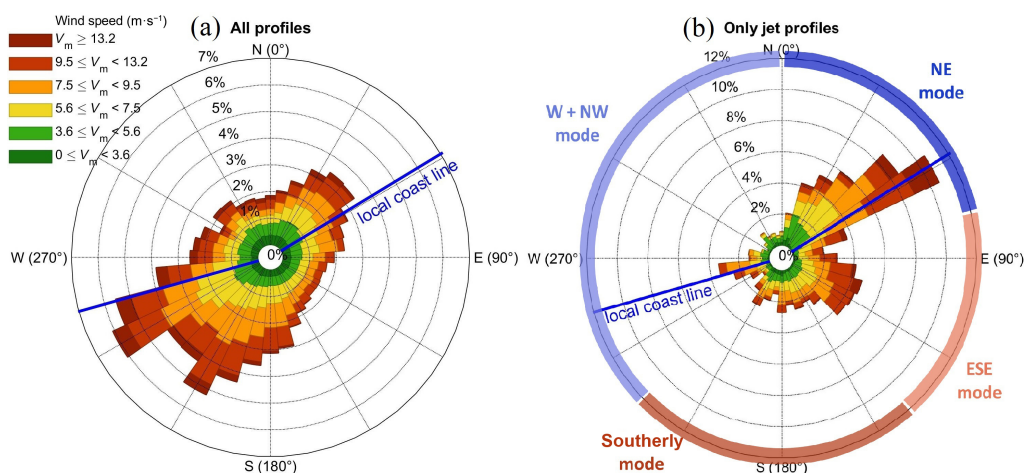


FIGURE 3 (a) General distribution of the wind direction at 114 m above the mean sea level and (b) distribution of the low-level jet (LLJ) core directions, plotted as wind roses using the six speed classes defined in Section 2.2 and pictured in Figure 2. In (a), the fractions are relative to the total number of wind profiles (227,694); in (b) the fractions are relative to the total number of wind profiles with a jet (11,462); the bins are 10° wide. The plain blue line represents the coastline direction in Dunkerque region, the sea/land being located above/below the line respectively. In (b), the outer circle indicates the angular domains corresponding to each of the four LLJ direction modes defined in Section 2.2 [Colour figure can be viewed at [wileyonlinelibrary.com](https://onlinelibrary.com)]

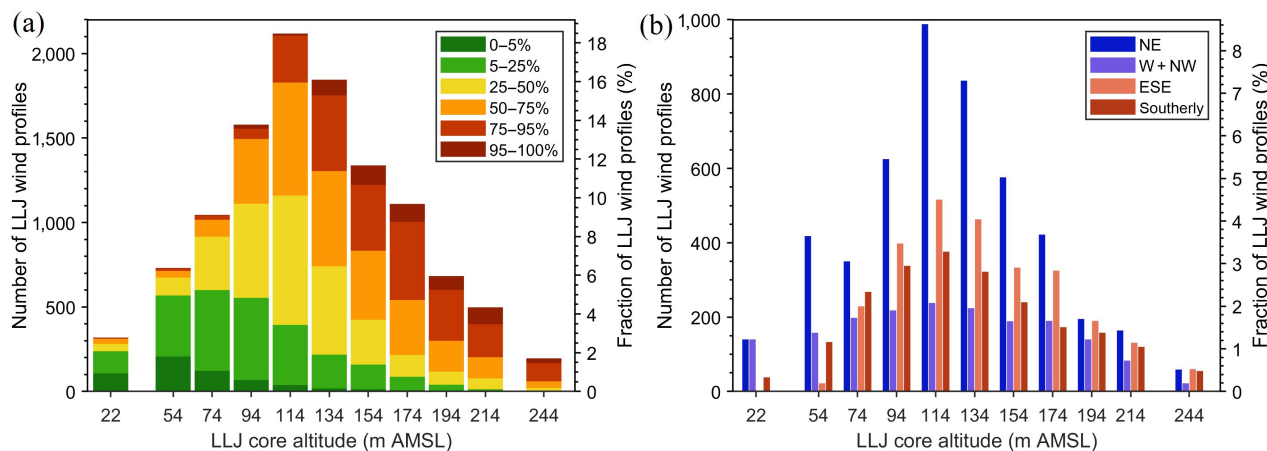


FIGURE 4 Distribution of the Low-Level Jet (LLJ) core heights by (a) speed classes and (b) direction mode, as defined in Section 2.2 and pictured in Figures 2 and 3b. The frequencies of occurrence are all relative to the total number of profiles selected (11,462). The lidar settings evolved with time, and the exact altitude of the lidar gates located above 200 m above the mean sea level (AMSL) changed; therefore, the rightmost bin gathers all values ≥ 234 m AMSL. As most of them were actually located at 244 m AMSL, the rightmost bin is represented at this altitude [Colour figure can be viewed at [wileyonlinelibrary.com](https://onlinelibrary.wiley.com/doi/10.1002/qj.4480)]

In Dunkerque, a secondary mode in the LLJs' core direction existed, gathering offshore jets rotated 30° to 80° clockwise from the coastline (i.e., southeast to east). This “east-southeasterly mode”, ranging from 80° to 140° in direction, represented 23% of the total number of LLJ profiles and also contained a small but significant share of strong jets. The rest of the jet core rose was subdivided into two modes, separated by a sharp hollow in frequency in the southwest direction. From 140° to 225° in direction, the southerly mode corresponded to a plateau in the wind rose, gathering 19% of the LLJ profiles, mostly moderate jets. Finally, there was a minor peak in the west direction (coastwise, exiting the English Channel) and very few jets from the west-northwest to north direction; both were gathered in a “westerly + northwesterly mode”, which accounted for 16% of the LLJ profiles.

The daytime and nighttime jet core wind roses (Supporting Information Figure S2) show that the east-southeasterly and southerly (i.e., the offshore LLJ modes) were dominantly nocturnal (with, respectively, 77% and 70% of the wind profiles in these modes being recorded during the night). On the contrary, the northeasterly (i.e., onshore coastwise mode) was even more dominantly diurnal (at 82%). For the westerly + northwesterly (onshore) mode, the westerly jets (around 260°) were dominantly nocturnal, but the northwesterly jets (280 to 360°) were almost exclusively diurnal, resulting in a more balanced repartition with 58% of diurnal cases. This shows that the westerly + northwesterly mode very likely gathered two different types of jets. The latter were still grouped in a single mode because, even together, they represented only a minor fraction of the jets. The LLJ diurnal cycle will be discussed in more detail in Section 3.3.2.

3.2.3 | Jet core height

The distribution of the LLJs' core altitudes retrieved over Dunkerque during the whole period is presented in Figure 4a. The most common jet core height was 114 m AMSL, the general distribution being rather symmetric around this altitude. A large majority (79%) of the jets' cores were located between 74 and 174 m AMSL, whereas very few jets had a core height really close to the surface (2.8% at 22 m AMSL), and even fewer were located at the highest altitude where they can be detected (1.2% ≥ 234 m AMSL). The core altitudes above 200 m AMSL were accessible during only 77% of the record (Section 2.1), so they might be slightly underrepresented; also, having higher observations would allow the detection of more elevated jets. However, the number of LLJ wind profiles observed at the highest accessible altitudes represented only a small share of the total, and comparison with the two sites closest to Dunkerque suggests that the peak altitude would not change upon extending the range of the observations (Section 4).

The details of the distribution by speed class show that the core height tended to increase with increasing core speed. The weak jets were the most frequent at 54 m AMSL, and their frequency steadily decreased with increasing altitude; none was found above 200 m AMSL. On the contrary, the strong jets were most frequent between 134 and 174 m AMSL and represented the majority of the cases with a core height above 200 m AMSL. This behavior can be visualized in more detail when looking at the core speed range observed at each possible core height (Supporting Information Figure S3): the median jet core height grew with increasing core speed

from $\sim 4.5 \text{ m}\cdot\text{s}^{-1}$ at 54 m AMSL to $\sim 11 \text{ m}\cdot\text{s}^{-1}$ above 200 m AMSL.

Figure 4b presents the distributions of LLJ core heights computed for the four direction modes separately. All modes, except the westerly one, had their most frequent core altitude at 114 m AMSL, like the general distribution. However, the height distribution of the offshore modes (southeasterly and easterly) was skewed toward slightly higher core altitudes compared to the dominant northeasterly mode. The westerly mode had a flat distribution with a broad peak from 74 to 134 m AMSL. In the end, the low core altitudes (22 and 54 m AMSL) were dominantly associated with onshore jets, whereas the highest core altitudes (194 m AMSL and above) had a fraction of offshore jets larger than the general ensemble. Nevertheless, the core speed varied in a similar way with the core height for the northeasterly (onshore) and eastsoutheasterly (offshore) jets, at least in the part of the profile with enough points to compute reliable statistics (Supporting Information Figure S3) and this, even though these two modes were respectively diurnal/nocturnal and occurred in different weather conditions (Section 3.4). One may think that the nocturnal offshore LLJs tended to have a higher core altitude because they developed in altitude from frictional decoupling, while northeasterly jets developed from the surface from the land–sea temperature gradient (sea breezes) or from the orography and land–sea surface roughness contrast (wind channeling jets). However, due to the inertial oscillation, an onshore jet can turn offshore in a few hours, so the jet core direction at the time of the observation is not a sufficient parameter

to fully discriminate between the LLJs' formation mechanisms and conclude about their influence on the core height.

3.2.4 | Shear and mixing below the jet

Figure 5a presents the distribution of the shear between the near surface (22 m AMSL) and the jet core in terms of wind speed. The maximum observed value was 0.22 s^{-1} , but the distribution was plotted only up to 0.13 s^{-1} because only eight cases (0.07%) fall above this value. The average and standard deviation of the shear in speed were $0.041 \pm 0.022 \text{ s}^{-1}$, which would correspond to a speed difference of $\sim 4 \text{ m}\cdot\text{s}^{-1}$ with the most frequent core height of $\sim 114 \text{ m}$ AMSL. The tail of the distribution stretched on the right-hand side up to 0.10 s^{-1} ; that is, speed differences $\sim 10 \text{ m}\cdot\text{s}^{-1}$. The distribution of the shear coefficient α corresponding to these values is presented in Supporting Information Figure S4a. Although it extended up to 2.8, the figure was cropped at 1.25 as only 54 values were larger, with the most frequent values being between 0.40 and 0.55.

Compared with the general distribution including all wind profiles, the distribution of speed shear values under LLJs was clearly shifted to the right (Figure 5a), which means that, on average, the shear increased in the presence of a jet. Globally, the northeasterly mode tended to generate lower shear values than the eastsoutheasterly mode; as this mode is not associated with lower core heights or weaker core speeds, this means it must have been associated with stronger surface winds below

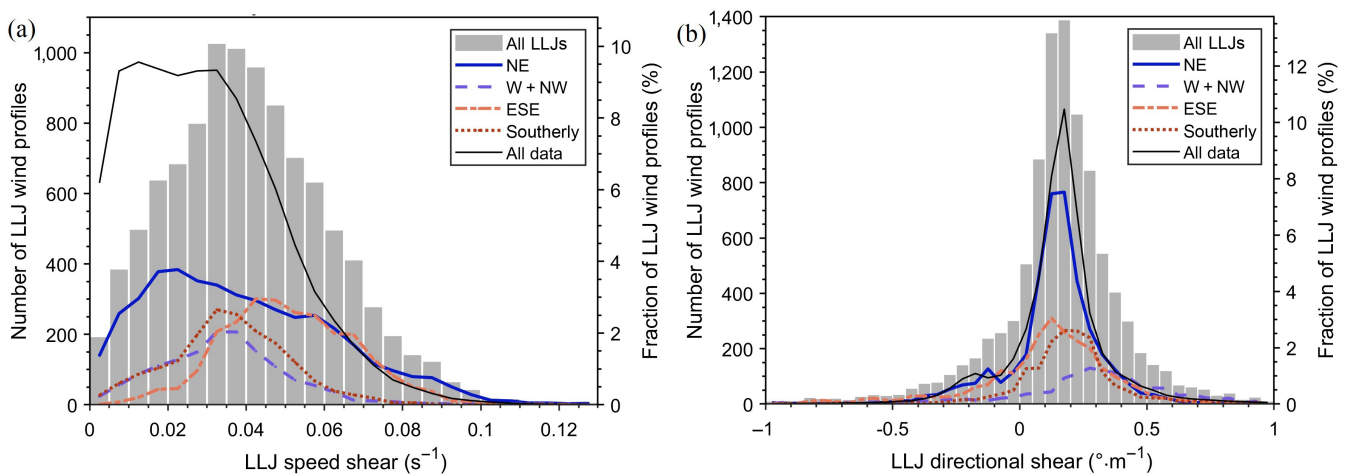


FIGURE 5 Distribution of the wind shear between the near surface (22 m above the mean sea level [AMSL]) and the jet core: (a) speed shear and (b) direction shear, detailed by direction mode as defined in Section 2.2. A positive shear means the wind veered clockwise with increasing altitude. The frequencies of occurrence are all relative to the total number of profiles with low-level jets (LLJs) that included a measurement from the sonic anemometer, for which the shear with the near surface could be determined (10,038). The black lines represent the distributions computed using all the data (with or without a jet) between 22 and 114 m above the mean sea level, and scaled so that the right y-axis scale remains correct; an additional one-half factor was applied in (b) as the distribution is very sharply peaked [Colour figure can be viewed at wileyonlinelibrary.com]

the jet. Indeed, under northeasterly LLJs, the ultrasonic anemometer provided higher values of the vertical turbulent intensity TI_w (vertical wind standard deviation normalized by the wind speed; Supporting Information Figure S4b). This means that the vertical mixing below the jet was stronger for the northeasterly mode than for the other three modes. Conversely, the offshore modes were associated with higher shear values and lower vertical mixing. This difference might only be due to the fact that the northeasterly mode was dominantly diurnal whereas the offshore modes were dominantly nocturnal, or result from frictional decoupling, if this mechanism was indeed the one driving a majority of the offshore jets. The general distribution of TI_w was shifted and stretched toward higher values compared with the distribution computed under LLJs only (Supporting Information Figure S4b); this means that jets do not increase the mixing compared with the all-time average. However, to determine whether LLJs enhance the vertical mixing or not, it would be more relevant to compare the turbulent intensity values retrieved just before and after the jet onset; that is, in similar synoptic conditions. In Supporting Information Figure S4b, the values measured in stormy conditions likely pull the distribution toward the high turbulent intensity values.

Figure 5b presents the distribution of the shear between the near surface and the jet core in terms of wind direction. The directional shear ranged from -11.0 to $+10.9^\circ \cdot \text{m}^{-1}$, but the distribution was plotted only between $-1^\circ \cdot \text{m}^{-1}$ and $+1^\circ \cdot \text{m}^{-1}$ because 84% of the values fell in this interval. The shear in direction peaks around $+0.15^\circ \cdot \text{m}^{-1}$, with 70% of the values lying between -0.15 and $+0.45^\circ \cdot \text{m}^{-1}$. The distribution was skewed toward positive values (clockwise rotation with increasing altitude), as can be expected due to the Coriolis effect, and this veering tended to be more pronounced for the southerly and the westerly + northwesterly LLJ modes. Compared with the general distribution including all wind profiles, the distribution of directional shear values under LLJs was much wider, which means that, on average, the wind direction veering increased in the presence of a jet. Both veering directions were represented, though the clockwise rotation was favored.

3.3 | Jet temporal variability

3.3.1 | Seasonal and annual cycles

The distribution of the jet profiles by season (Figure 6a) shows that LLJs were the most frequent in summer, closely followed by spring (about 38 and 35% of the total number of wind profiles with jet, respectively). LLJs were twice less frequent in autumn (19%), which was

an intermediate season, and even four times less frequent in winter (9% of the total). The share of strong jets was also significantly higher in spring, compared with the other seasons. The seasonal distribution detailed by direction mode (Figure 6c) shows that the amplitude of the seasonal cycle was even more pronounced when considering only the northeasterly mode (onshore coastwise), which was almost absent during winter. One could expect the two onshore modes (northeasterly and westerly + northwesterly) and the two offshore modes (east-southeasterly and southerly) to exhibit a similar behavior. However, the minor onshore mode (westerly + northwesterly) peaked in summer instead of spring, though, as with the northeasterly mode, it was very rare in winter and uncommon in autumn. Regarding the offshore modes, the east-southeasterly mode exhibited a seasonal cycle similar to the northeasterly mode, though with a much smaller amplitude, whereas the southerly mode behaved completely differently from the other three. This mode was the most frequent in autumn, then winter, and the least frequent in summer.

The annual cycle of the LLJ occurrence (Figure 6b) shows that very marked month-to-month differences existed inside a given season, and that the annual cycle did not have a smooth shape. The high LLJ season actually extended from April to August, with the months of April, May, and August standing out; April also had a significantly larger share of the strongest jets. On the contrary, the number of LLJs was at its lowest in February. The annual cycle detailed by direction mode (Figure 6d) shows that the northeasterly mode occurred from March to September only (with a marked peak value in April, and a relative pause in July), but this mode was almost non-existent during the cold months, from October to February. The other onshore mode (westerly + northwesterly) also occurred significantly from March to September, but with a different month-to-month behavior (it peaked from May to August but was still rare in April). The southerly mode, on the contrary, had its highest occurrences from October to January, peaking in November and December.

3.3.2 | Diurnal cycle

The diurnal cycle of LLJ occurrences (Figure 7, bar plot envelope) exhibited two marked peaks of similar amplitude: one in the late night (0000 to 0700 UTC) and one in the afternoon (1200 to 1800 UTC), gathering respectively 39% and 31% of the wind profiles with jets. On the contrary, the LLJ diurnal cycle exhibited a marked minimum during the late morning, with only 6% of the cases occurring between 0800 and 1100 UTC. During the evening and

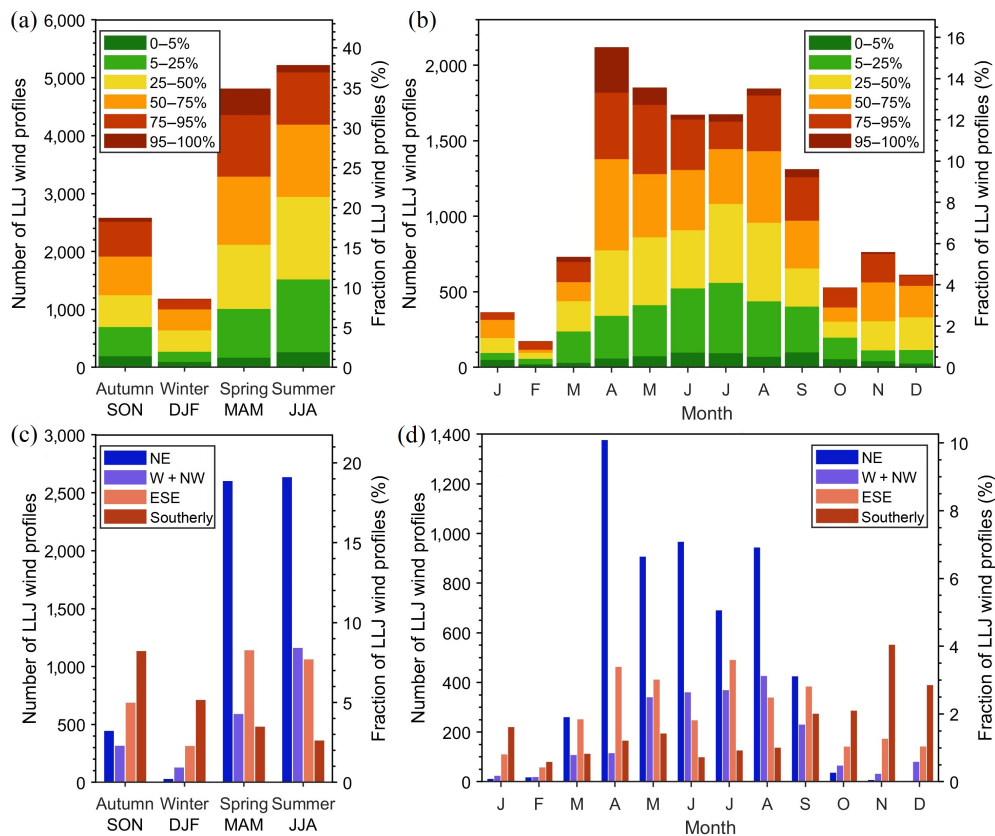


FIGURE 6 Seasonal and annual cycles of low-level jet (LLJ) occurrences (a, b) by speed class and (c, d) by direction mode, as defined in Section 2.2 and pictured in Figures 2 and 3b. The values are corrected for the variations in the seasonal and monthly data availability, as explained in Section 2.1 [Colour figure can be viewed at wileyonlinelibrary.com]

early night (1800 to 2400 UTC), the LLJ frequency followed a plateau of intermediate values. The weak jets (first quartile of the speed distribution) clearly peaked from 1100 to 1300 UTC, ahead of the afternoon LLJ peak, possibly because the core speed was weaker at the onset of the afternoon LLJ events. Conversely, the strongest jets (95th to 100th percentiles) peaked 1 hr later than the main peak (1300–1900 UTC), possibly because these values were recorded in well-established LLJs.

The frequencies of occurrence according to the four direction modes are detailed in Figure 7b. This clearly shows that the afternoon peak in LLJ frequency was mostly due to the northeasterly mode, whereas the late night peak was due to the two offshore modes (east-southeasterly and southerly) with an equal share. The evening and early night plateau results from a combination of the northeasterly mode persistence in the evening and the east-southeasterly mode increase from the early night. The westerly + northwesterly mode daily cycle is more or less constant, which confirms that this mode might actually gather different types of LLJs.

3.3.3 | Jet events' durations

Using the 3-hr time-continuity criterion (Section 2.2), the 11,462 wind profiles with jets were gathered into 769

events. The performance of the grouping process was assessed by plotting time series of the jet core direction and jet event number over the whole period of study (an example is provided in Supporting Information Figure S5). The jet core direction was used to ensure that events of a different nature separated by a short time interval were not mixed (e.g., May 24 in Supporting Information Figure S5); a slow rotation of the jet core direction was, of course, allowed during a single event.

The longest jet event detected lasted for 26 hr 20 min, and another one lasting 20 hr 50 min was found. However, most events were much shorter, and the average duration was 3.1 hr with a standard deviation of 3.7 hr. Figure 8 presents the distribution of the jet events' durations with irregular bins on the left-hand side, to give more details about the probabilities of short events. The frequency of occurrence of the events steadily decreased with increasing duration, reaching zero for an event duration of 18 hr (the two extra events are not represented here). Among the 769 events detected, 18% were very short and lasted only 20 min (this is the minimum for LLJ detection), 19% lasted from 30 to 50 min, 17% lasted from 1 to 2 hr, which leaves 46% of events lasting more than 2 hr. Distinguishing the events by direction would be interesting to see which type lasted longer, but the jet can change direction completely during a single event, with a continuous turn, so it did not make sense to attribute a jet event to

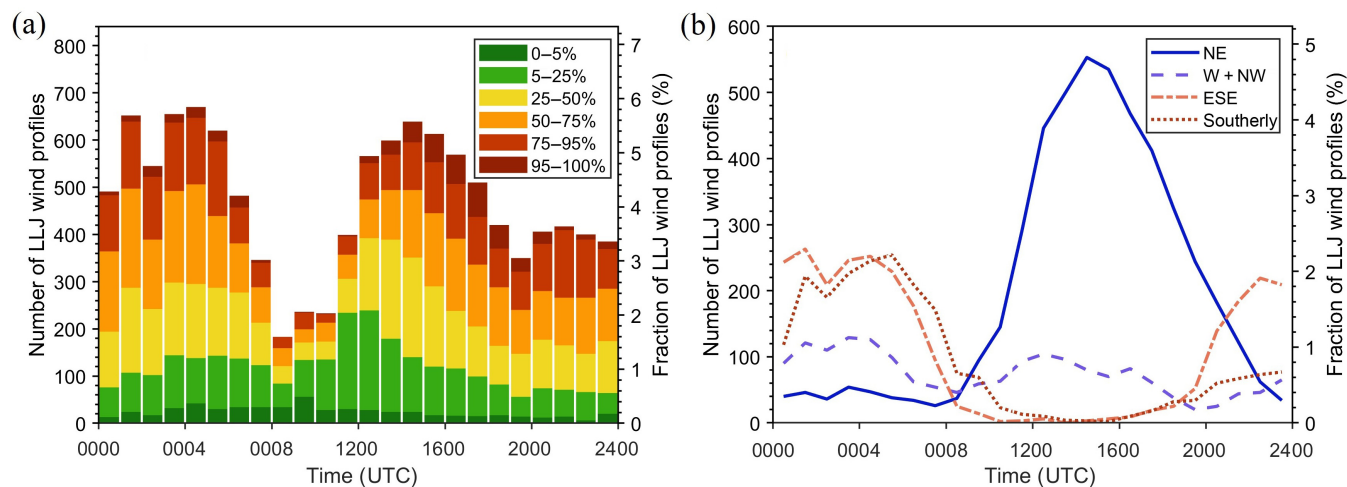


FIGURE 7 Diurnal variation in low-level jet (LLJ) occurrences (a) by speed class and (b) by direction mode, as defined in Section 2.2 and pictured in Figures 2 and 3b. All frequencies are relative to the total number of wind profiles with a jet (11,462) [Colour figure can be viewed at wileyonlinelibrary.com]

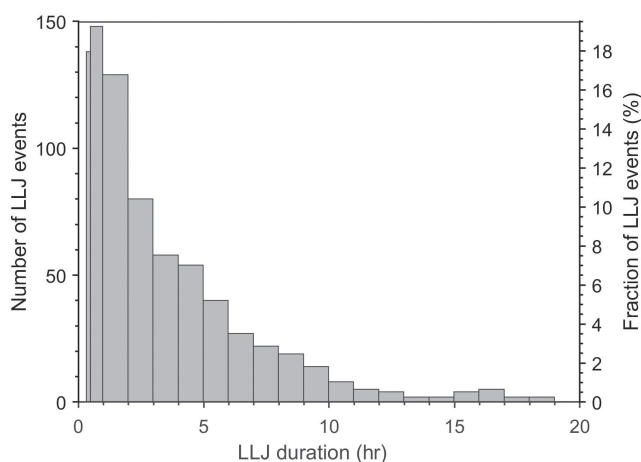


FIGURE 8 Distribution of low-level jet (LLJ) event durations. In order to distinguish the probability of the shortest events, the first two bins are narrower (20 min and 30–50 min). The frequencies are relative to the total number of events found (769)

a given direction mode. The number and duration of the events varied along the year following a seasonal cycle (not shown) similar to the one obtained before grouping the jet profiles into events.

3.4 | Weather conditions favoring jet occurrence

3.4.1 | Land–sea thermal contrast

Figure 9 presents the general distribution of the temperature difference between land and sea in the Dunkerque region, as defined in Section 2.3. This distribution is skewed toward negative values, meaning that the air over the southern Flanders Plain is more often colder than the

air over the southern North Sea, with most values comprised between -4 K and $+3$ K. Figure 9 also presents the same distribution computed using only the values interpolated at the time of LLJ wind profiles and distinguishing the four direction modes defined in Section 2.2. The distribution for the northeasterly mode was very different from the general one, with a flat plateau between -1 K and $+7.5$ K, indicating that a land warmer than the sea was a driving factor for the formation of northeasterly jets. This follows the daily and annual cycle of the northeasterly LLJs, which occurred dominantly during the afternoon (Figure 7) and almost exclusively from March to September (Figure 6d) when the solar flux was strong enough to warm up the land. The annual cycle of the land–sea temperature difference observed during LLJs shows that the land–sea temperature difference was clearly more positive during northeasterly LLJs (Figure S6a), with monthly average values higher by 2.5–3.5 K than the overall monthly average.

A small share of the onshore jet cases was associated with slightly negative temperature gradient values; that is, with a land slightly colder than the sea. Indeed, Figure 9 was built using the temperature difference at the time of the LLJ wind profiles, not the one prevailing at the onset of the jet events. Consequently, if the jet event is still ongoing at sunset, the sign of the temperature gradient may change as a result of the faster radiative cooling over land, just before that puts an end to the onshore jet. This can be confirmed by the daily cycle of the land–sea temperature difference for the four LLJ modes (Supporting Information Figure S6b): the northeasterly cases with a slightly warmer sea clearly occurred during the night.

Here, we refrain from using the locution “sea breeze” because northeasterly diurnal jet events may be associated

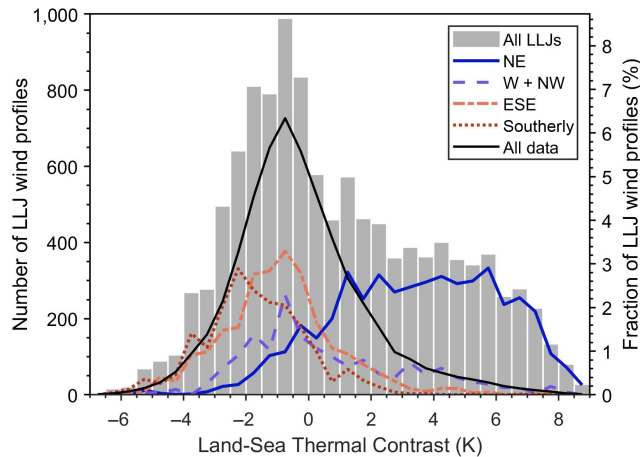


FIGURE 9 Distribution of the land minus sea temperature difference in the Dunkerque region (Section 2.3), computed using the ERA5 values interpolated at the time of low-level jet (LLJ) profiles, separating the four direction modes defined in Section 2.2. The black line represents the distribution computed using all the hourly ERA5 data from July 1, 2016, to September 30, 2021, and scaled so that the right y-axis scale can be used (an additional one-half factor was applied, as the all-data distribution was more peaked) [Colour figure can be viewed at [wileyonlinelibrary.com](https://onlinelibrary.wiley.com)]

with a regional circulation extending over the whole Dover Strait (Capon, 2003); this type of event may occur when a northeasterly geostrophic flow is channeled by the orography, an effect that combines with the surface roughness contrast between land and sea. It is possible that the coastwise northeasterly mode would correspond to regional jet events whereas the northwesterly jets in the westerly + northwesterly mode, which are more perpendicular to the coastline, would better correspond to local sea breeze events. Indeed, the daytime cases of westerly + northwesterly LLJs, which are mainly northwesterly (Section 3.2.2), do correspond to a positive land–sea temperature difference (Supporting Information Figure S6b). However, distinguishing local sea breeze events from regional jets would require a more extensive use of reanalysis data and modeling studies that are out of the scope of the current work.

On the contrary, offshore jets (east-southeasterly and southerly) occurred mostly when the air over land was colder (from -4.0 K to $+0.5$ K). Throughout the year, the monthly average temperature difference was about 1 K colder under offshore jets than the overall monthly average (Supporting Information Figure S6a). This follows the daily cycle of those jets, which occurred dominantly at night, when the land cools faster than the sea. Here again, the small share of the offshore jets that were associated with slightly positive temperature gradient values could correspond to the end of the events, when the sun rises and warms the land faster than the sea. The few

daytime cases of offshore jets occurred during periods with a colder land (Supporting Information Figure S6b). As for the onshore jets, we refrain from using the locution “land breeze” because the distinction between local and regional phenomena was not made at this stage.

3.4.2 | Atmospheric stability

Figure 10a presents the general distribution of the Pasquill atmospheric stability classes in Dunkerque. Regarding the wind profiles, 43% were associated with “neutral” conditions (class D) and another 31% with “slightly unstable” conditions (class C), which is coherent with the fact that a coastal area is rarely exposed to strongly stable or strongly unstable conditions. Figure 10b presents the same distribution but computed only using data coinciding with LLJ wind profiles and separating the four direction modes. LLJs from the dominant onshore coastwise mode (northeasterly) were observed under all stability conditions; however, compared with the general distribution, the “moderately unstable” and “extremely unstable” conditions (classes B and A respectively) were overrepresented. This was not so clear for the minor onshore mode (westerly + northwesterly), which occurred preferentially under “slightly stable” conditions (class C).

On the contrary, the offshore jets were favored by “neutral”, “moderately stable”, and “extremely stable” conditions (classes D, E, and F respectively) and almost never occurred under “extremely unstable” or “moderately unstable” conditions (classes A and B respectively). This is coherent with the fact that these jets occurred dominantly during the night (Sections 3.2.2 and 3.3.2) and generated lower vertical mixing at the surface (Section 3.2.4), all facts that point toward frictional decoupling as their formation mechanism. However, if some of the jet events’ hodographs did show the clockwise veering of the core direction expected from the inertial oscillation, a large share of them, if not the majority, exhibited a core direction that remained stable in time or oscillated around a central value (Supporting Information Figure S7). This means that frictional decoupling/inertial oscillation was not the only mechanism responsible for the offshore nocturnal jets.

3.4.3 | Geostrophic flow

Figure 11a presents the wind rose of the geostrophic wind in the Dunkerque region, computed from the geopotential gradient at 850 hPa, as detailed in Section 2.3. The strongest geostrophic winds (≥ 10 m s $^{-1}$) represented 44% of the data and were observed mainly from the west to southwest directions. Those directions were also the

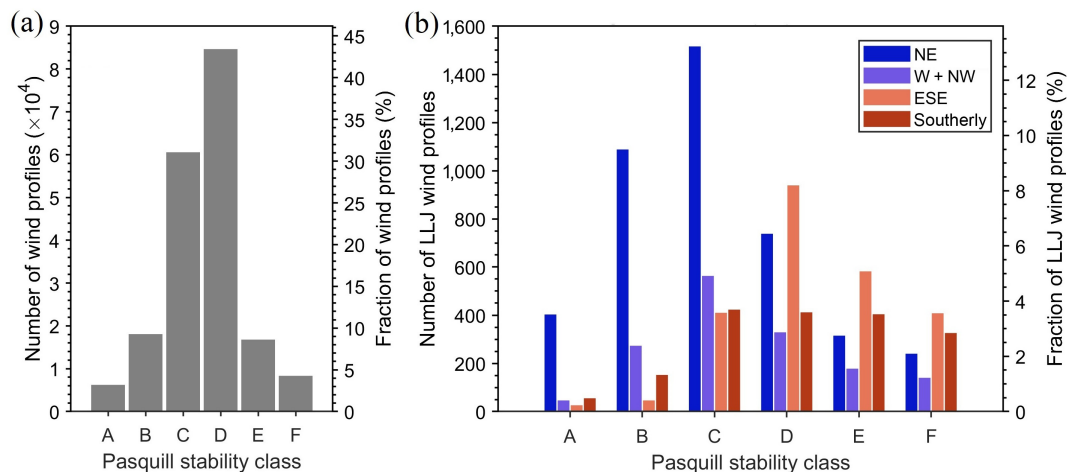


FIGURE 10 Distribution of the Pasquill atmospheric stability classes in Dunkerque, computed using (a) all the wind profiles including ultrasonic anemometer data (194,925 wind profiles) and (b) only the wind profiles with a low-level jet (LLJ) and ultrasonic anemometer data (10,038), and separating the four direction modes defined in Section 2.2. The boundaries of the stability classes are defined as explained in Section 2.3. The A to F stability classes correspond respectively to “extremely unstable”, “moderately unstable”, “slightly unstable”, “neutral”, “moderately stable”, and “extremely stable” conditions [Colour figure can be viewed at [wileyonlinelibrary.com](https://onlinelibrary.wiley.com/doi/10.1002/qj.4480)]

most frequent wind origins and correspond to the passage of cyclonic systems bringing oceanic air masses over the Dunkerque area. For 14% of the cases, the geostrophic wind was very low ($<4 \text{ m}\cdot\text{s}^{-1}$), which corresponds to the stagnant conditions occurring under a high-pressure center. Weaker continental flows from the northeast to south – that is, associated with anticyclonic conditions – were several times less frequent than the west to southwest oceanic flows. When considering only the data interpolated at the time of the LLJ wind profiles (Figure 11b), the share of variable winds increased to 41% whereas the share of strong geostrophic winds dropped to 7%, which means that stagnant conditions favored jet formation. Also, when selecting only the data coincident with a LLJ, the share of continental flows became comparable to the share of oceanic flows, which means that anticyclonic conditions were favorable for jet formation and that cyclonic conditions were unfavorable.

The geostrophic wind roses plotted separately for each of the four direction modes are presented in Figure 12. The northeasterly and eastsoutheasterly LLJ modes were clearly associated with anticyclonic conditions (Figure 12b,c respectively), with a higher share of stagnant conditions ($<4 \text{ m}\cdot\text{s}^{-1}$) and the rest corresponding to gentle continental flows from the southeast quadrant. This is especially the case for the northeasterly mode, with 50% of the profiles belonging to this mode recorded under stagnant conditions, which does not really support the flow channeling hypothesis. However, the lower altitude geostrophic wind roses (not shown) do exhibit easterly flows, so a more extensive study of this type of jet is required to better understand its formation

mechanism. Regarding the onshore cross-coast eastsoutheasterly mode, which occurred more frequently in spring and summer (Section 3.3.1) and was mostly nocturnal (Section 3.3.2), it could be associated with the land breeze phenomenon. However, the two main types of hodographs observed for the eastsoutheasterly mode (Supporting Information Figure S7) suggest that it also included jets formed from frictional decoupling: when the air in altitude is isolated from the ground due to the nocturnal temperature inversion, this air accelerates as it is no longer slowed by turbulence generated by friction on the ground.

Conversely, the southerly and westerly + northwesterly LLJ modes were clearly associated with cyclonic conditions (Figure 12a,c respectively), with a higher share of stronger geostrophic winds ($>8 \text{ m}\cdot\text{s}^{-1}$) and a dominance of southwesterly to westerly directions. In particular, the southerly mode was associated with the strongest geostrophic winds and a narrow family of wind directions from the southwest. Also, the southerly LLJ mode occurred preferentially during winter (Section 3.3.1), so that it might be associated with winter storms passing over the region and correspond to the type of jet that appears ahead of a cold front. Regarding the westerly + northwesterly LLJ mode, it was associated with more dispersed geostrophic wind directions (Figure 12a). When separating the daytime and nighttime cases (not shown), it appears that the westerly jets (dominantly nocturnal) were mostly associated with west to west-southwest geostrophic flows, whereas jets from the rest of the northwest sector (mostly diurnal) occurred mostly under stagnant conditions. Westerly jets, whose direction corresponds to the Channel exit, might, therefore,

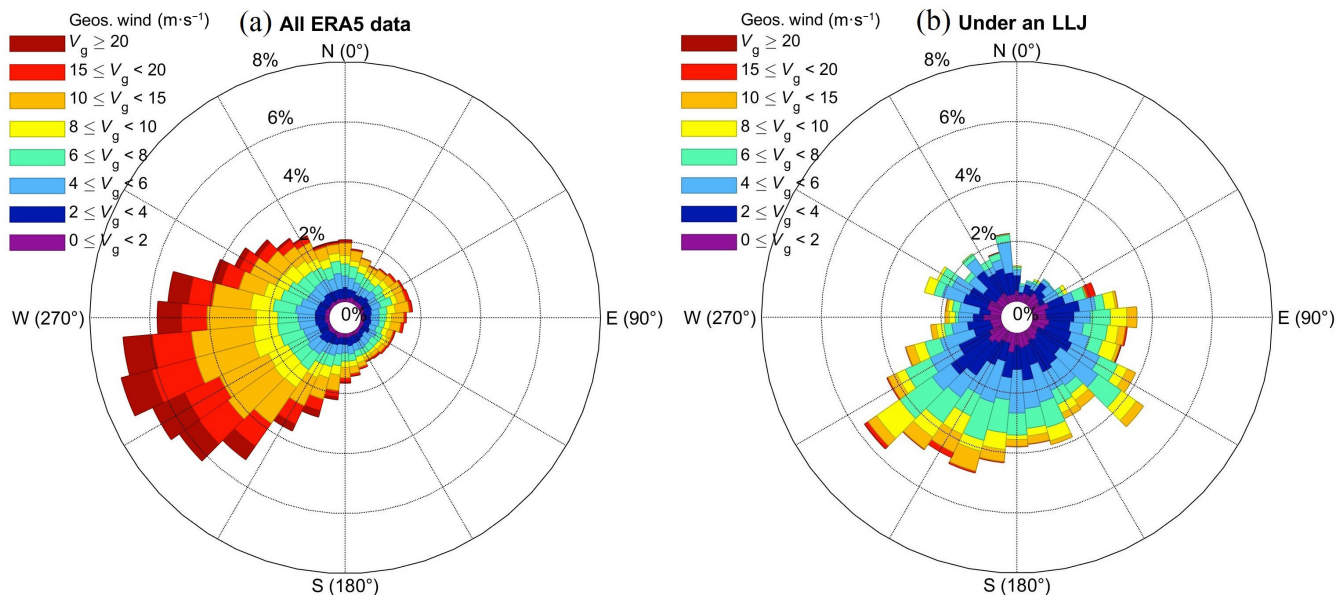


FIGURE 11 Wind rose of the geostrophic wind at 850 hPa over the Dunkerque region (Section 2.3), computed using (a) all the hourly ERA5 data and (b) the values interpolated at the time of the low-level jet (LLJ) profiles [Colour figure can be viewed at [wileyonlinelibrary.com](https://onlinelibrary.wiley.com/doi/10.1002/qj.4480)]

be the counterpart of northeasterly jets and result from westerly wind channeling in the Dover Strait, whereas northwesterly jets more likely sea breezes.

4 | DISCUSSION

In this section, we compare our results mainly with other studies performed in the North Sea area: on the inland sites of Cabauw (Baas *et al.*, 2009), WiValdi (Wildmann *et al.*, 2022) and Braunschweig (Ziemann *et al.*, 2020), on the offshore platforms of IJmuiden (Duncan, 2018; Kalverla *et al.*, 2017; Kalverla *et al.*, 2019) and FINO1 (Wagner *et al.*, 2019a). Cabauw is located ~ 50 km from the sea and ~ 205 km to the eastnortheast from Dunkerque (Figure 1a); for wind profiling, the site was equipped with a 200 m meteorological tower and a radio-acoustic sounding system; the LLJ climatology in Cabauw is very robust, as it relies on 7 years of wind profiles (Baas *et al.*, 2009). The WiValdi site is located ~ 40 km inland and ~ 560 km northeast from Dunkerque; a wind lidar covering the whole boundary layer was deployed there and 16 months of data were used to produce a first climatology of the jets (Wildmann *et al.*, 2022). The Braunschweig site is located way farther inland (~ 170 km) also ~ 560 km from Dunkerque but to the eastnortheast; it was equipped with a Doppler lidar reaching up to 500 m AGL; however, only observations from the three summer months were published (Ziemann *et al.*, 2020). The FINO1 platform is located ~ 40 km from the German island of Bokrum and ~ 440 km to the northeast from Dunkerque (Figure 1a); it is equipped with

a meteorological mast and a long-range Doppler lidar (Wagner *et al.*, 2019a); the LLJ climatology in FINO1 is less robust, as it relies on only 1 year of data and with low overall data availability. The IJmuiden platform is located ~ 85 km from the Dutch coast and ~ 214 km to the north-northeast from Dunkerque (Figure 1a); it was equipped with a 90 m meteorological mast and 300 m range Doppler lidar; the LLJ climatology in IJmuiden is robust as it is based on 4 years of wind profiles (Kalverla *et al.*, 2017; Duncan, 2018). Kalverla *et al.* (2019) aggregated the data from seven offshore platforms in the Dutch part of the North Sea, including IJmuiden, and also analyzed 10 years of ERA5 data.

4.1 | Sensitivity to the detection criteria

Increasing the minimum number of consecutive wind profiles with a jet, adding core height or core direction continuity criteria, or requiring the wind to decrease also below the jet core are all changes that had similar effects on the properties of the LLJs retrieved. First, less weak jets were detected, especially with core speeds below $3.5 \text{ m}\cdot\text{s}^{-1}$, either because these were short-lived events or because the core speed may temporarily have fallen below the detection threshold. Consequently, the shear distribution was shifted toward slightly higher values. Second, less very low altitude jets were detected (at 22 and 54 m AMSL), which is not surprising as they correspond dominantly to weak jets (Figure 4). Less top-altitude jets were also retrieved when using longer time-continuity criteria, likely because the

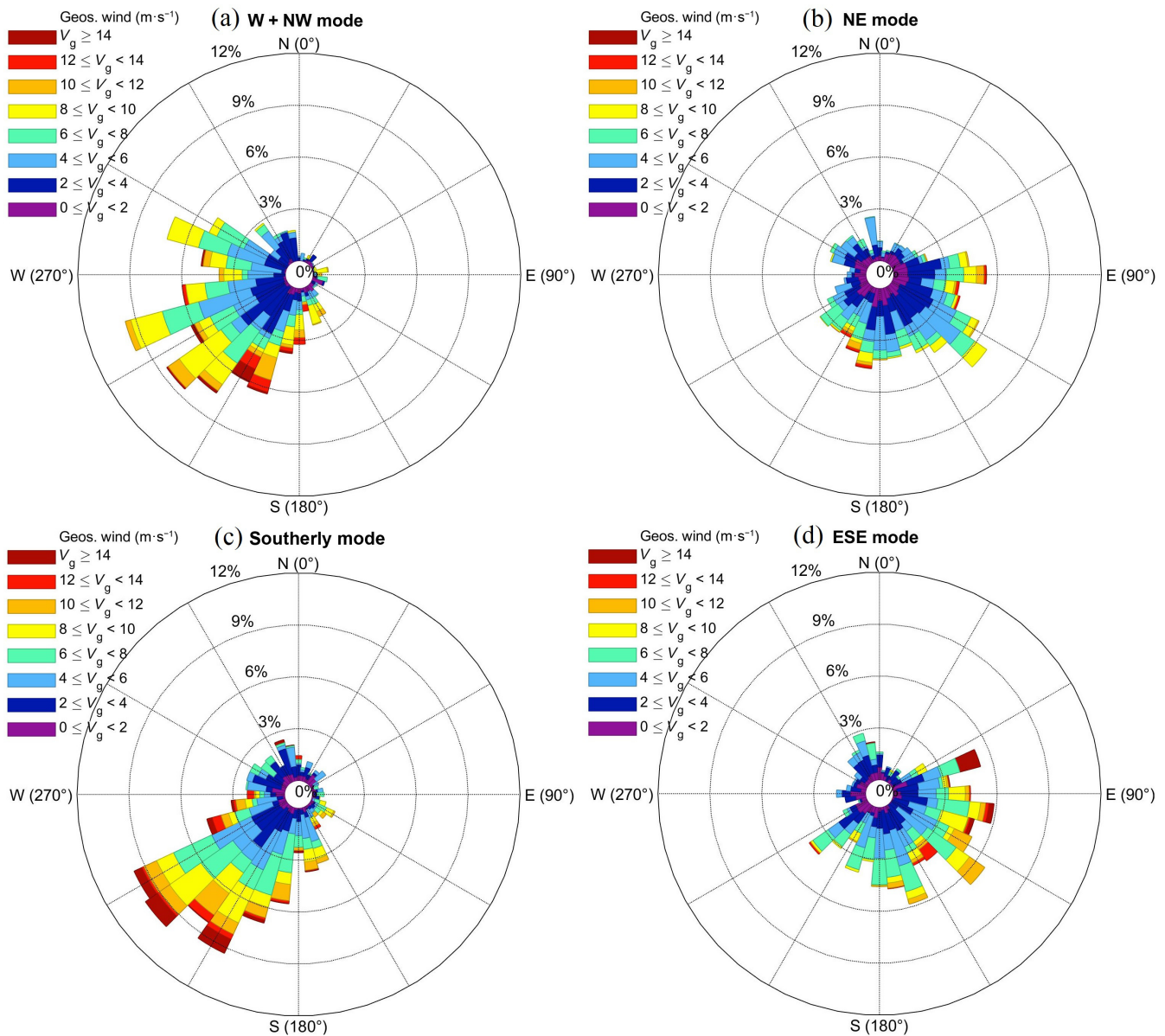


FIGURE 12 Wind rose of the geostrophic wind at 850 hPa over Dunkerque region (Section 2.3) computed using the values interpolated at the time of the low-level jet (LLJ) profiles for the four direction modes (as defined in Section 2.2): (a) westerly + northwesterly (W + NW) onshore mode, (b) northeasterly (NE) onshore mode, (c) southerly offshore mode, and (d) eastsoutheasterly (ESE) offshore mode. The results are expressed as a fraction (in percent) of the wind profiles in the corresponding LLJ mode [Colour figure can be viewed at wileyonlinelibrary.com]

core height temporarily rose above the maximum detection altitude. Third, LLJs from the northwest quadrant almost completely disappeared, which is coherent with these jets often being weak and very low-altitude LLJs. The westerly + northwesterly mode was thus reduced to coast-wise LLJs exiting the English Channel (Figure 3b). Fourth, the general shape of the annual and daily cycles was preserved, although the month-to-month or hour-to-hour variability was higher due to the reduced number of points included in the distributions. In particular, the number of jets detected during the months of May, June, and July was reduced more than during other months, due to the larger

share of weak jets occurring during these three months. As for the daily cycle, the depletion was more marked during the night, and particularly strong in the morning (few jets were left from 0800 to 1100 UTC), so the afternoon peak became more prominent. Fifth, the jets' conditions of occurrence became more coherent with the expectation: using longer time-continuity criteria reduced the numbers of LLJ cases occurring with an unexpected sign of the land–sea temperature difference (i.e., less cases with a warmer land for offshore jets and the reverse for onshore jets). It also reduced the number of westerly + northwesterly, eastsoutheasterly, and southerly jets

occurring under the three unstable classes, so that unstable conditions were almost exclusively associated with the northeasterly mode, whereas the three other modes were dominantly associated with neutral and stable conditions. Finally, the 850 hPa geostrophic flows under which the jets occurred were similar for the different continuity criteria; imposing longer time-continuity periods only increased the share of stagnant conditions by a few percent (and conversely for the strong geostrophic flows).

4.2 | Core speed

The core speed distribution retrieved over Dunkerque (Figure 2) is very similar to the ones presented for the two inland sites that are located not too far from the North Sea; that is, Cabauw (Baas *et al.*, 2009) and WiValdi (Wildmann *et al.*, 2022): they all showed the same asymmetric shape, with peak values around $8 \text{ m}\cdot\text{s}^{-1}$, though the inland speed distributions extended up to higher wind speeds. On the IJmuiden offshore platform, the core wind frequencies also peaked around $8 \text{ m}\cdot\text{s}^{-1}$, but the shape of the distribution was different, with a larger number of strong wind values in the $10\text{--}20 \text{ m}\cdot\text{s}^{-1}$ range and the distribution's right wing extending up to $25 \text{ m}\cdot\text{s}^{-1}$ (Kalverla *et al.*, 2019). Wagner *et al.* (2019b) do not provide a core speed distribution for the FINO1 offshore platform, but they report a median core speed of $10.5 \text{ m}\cdot\text{s}^{-1}$ against $7.6 \text{ m}\cdot\text{s}^{-1}$ in Dunkerque, and extreme values up to $46 \text{ m}\cdot\text{s}^{-1}$, so the winds in FINO1 were also stronger than in the coastal site of Dunkerque. The larger number of high and extreme values of wind speed observed over the other sites might be due to a higher vertical extension of the observations, as more elevated jets tend to be faster (Section 3.2.3). Conversely, the lower number of weak wind speeds likely resulted from longer minimum duration criteria.

4.3 | Core direction

For the Cabauw inland site, Baas *et al.* (2009) present the jet direction distribution directly in term of geostrophic wind, so a comparison with the real core direction is not straightforward. At the other site closest to Dunkerque (IJmuiden), Duncan (2018) found two dominant modes for the LLJ core direction: from the north to northeast, and from the southsouthwest. The northnortheasterly mode in IJmuiden was not oriented exactly as the northeasterly mode found in Dunkerque, but this might come from differences in the coast orientation. Farther away from the English Channel, above sites located in northern Germany, northeasterly jets were not observed at all. This indicates that the IJmuiden site is potentially close

enough to the English Channel to be affected by wind channeling effects, whereas sites located farther on the Dutch and German coast are not. Conversely, the south-southwesterly LLJ mode found over IJmuiden, a direction that is associated with storm passages in the region, was also observed at the WiValdi inland site (Wildmann *et al.*, 2022) and at the FINO1 offshore platform (Wagner *et al.*, 2019a), but not significantly above Dunkerque. One possible explanation is that we missed part of these LLJs because, according to Duncan (2018), these jets tend to be located at slightly higher altitudes, and the observations at IJmuiden extended slightly higher than in Dunkerque. This higher altitude of southwesterly jets was confirmed by Wagner *et al.* (2019b) above the FINO1 offshore platform. In Cabauw, Baas *et al.* (2009) showed that southwesterly jets included the largest number of strong winds and that strong winds were associated with more elevated jets, so that we can suppose that southwesterly jets were generally more elevated in Cabauw too. Aside from the southwesterly mode, the jet core peaked respectively in the eastsoutheasterly and southeasterly directions at the WiValdi inland site (Wildmann *et al.*, 2022) and at the FINO1 offshore platform (Wagner *et al.*, 2019a), corresponding to cross-coast offshore jets like the eastsoutheasterly and southerly modes in Dunkerque. This would correspond to eastsoutheasterly to southeasterly jets in IJmuiden, a direction that was actually rare in the jet core rose (Duncan, 2018). Maybe this is because IJmuiden is farther from the coast than FINO1, and thus not impacted by jets formed over land.

4.4 | Core height

The distribution of jet core heights above the two sites closest to Dunkerque also peaked at low altitudes: around 100 m in IJmuiden (offshore; Kalverla *et al.*, 2019) and slightly higher, around 140 m, in Cabauw (inland; Baas *et al.*, 2009) against 114 m in Dunkerque. In Cabauw, though, the vertical resolution was coarser, so a precise comparison is not possible. However, for all sites located farther away from Dunkerque to the northeast, jets appear to be more elevated. Above the FINO1 offshore platform, the most frequent jet core height was around 240 m (Wagner *et al.*, 2019a). At Braunschweig inland site, the core height distribution (which covers only summer) peaked around 280 m, though a secondary maximum existed at 100 m (Ziemann *et al.*, 2020). No core height distribution is provided for the WiValdi inland site, but Wildmann *et al.* (2022) reported an even higher average altitude of $\sim 400 \text{ m}$, noting they could not detect jets below 100 m. Moreover, all these studies found jets up to the maximum altitude where they could be detected; that

is, up to 300–600 m, depending on the site. This is also true for the sites located closest to Dunkerque, where the jet core peaked at low altitude, which suggests that extending the range of observations in Dunkerque would allow detection of more elevated jets, though the most frequent core height would likely remain around 100 m, like in IJmuiden and Cabauw. Regarding the relationship between the jet core height and core speed, our results are very similar to the curve of Baas *et al.* (2009) for Cabauw, which is the only site for which such a plot is presented.

4.5 | Surface-to-core shear

Among the studies previously cited, the shear between the jet nose and the near surface is presented only for the FINO1 platform (Wagner *et al.*, 2019a), but the values are expected to be lower because the shear was computed using a higher reference altitude (33 m instead of 22 m AMSL). One common fact, however, is that LLJs from the continent (southeasterly direction) have stronger shear values both in FINO1 and in Dunkerque (east-southeasterly mode in Figure 5a). As said in Section 3.2.4, this could be a consequence of the frictional decoupling from the ground.

4.6 | Annual cycle

The cycle observed in Dunkerque is roughly similar to the one observed at IJmuiden (Kalverla *et al.*, 2017; Kalverla *et al.*, 2019) and Cabauw (Baas *et al.*, 2009), with a jet high season extending from March/April to September. However, the highest jet frequencies were observed at the beginning and end of the season in Dunkerque (April and August) but in the middle of the season (May–July) in IJmuiden (Kalverla *et al.*, 2017, Kalverla *et al.*, 2019) and rather at the end (July and August) in Cabauw (Baas *et al.*, 2009). This difference is a robust feature, because in Dunkerque the prevalence of the April and August months was reinforced when imposing stricter detection criteria, and statistics on the three sites all rely on long-term datasets. One possible explanation for the April peak in Dunkerque might be that, due to thermal inertia, the sea water remains very cold until May/June, whereas episodes with warm air temperature can already be observed in the early spring. The contrast between the sea-surface temperature and the air temperature is therefore stronger in spring than in summer, generating stronger and more frequent breezes; this would also explain why the fraction of strong jets is, by far, the highest in April. The annual cycle was not shown for the WiValdi site (Wildmann *et al.*, 2022)

or the FINO1 platform (Wagner *et al.*, 2019a), but the annual cycle observed in IJmuiden is similar to what was retrieved in the central Baltic Sea (Hallgren *et al.*, 2022) and on the US East Coast (Aird *et al.*, 2022).

4.7 | Daily cycle

The cycle obtained in Dunkerque is very different from the ones observed both inland and offshore. Above Cabauw, Baas *et al.* (2009) reported a nocturnal flat maximum roughly extending from 2100 to 0600 UTC, and a daytime flat minimum roughly extending from 0830 to 1800 UTC, with a behavior that is similar for weak and strong LLJs. Above the IJmuiden platform, Kalverla *et al.* (2017) also observed a nocturnal maximum and daytime minimum. The statistics from ERA5 gave the same kind of LLJ daily cycle (Kalverla *et al.*, 2019), though observing finely the figures suggests that, for the model, the daily minimum might last shorter for the southern stations that are located closer to Dunkerque than IJmuiden (very roughly, the period with fewer LLJs seems to extend only from 0800 to 1200 UTC instead of 0800 to 1500 UTC). More to the north, above the FINO1 platform, there was also a daytime minimum of LLJs, but it occurred later, from 1200 to 1700 UTC. In the end, the afternoon peak in LLJ occurrence observed in Dunkerque existed neither inland nor offshore, which suggests that it is related to a jet formation mechanism peculiar to the coastal environment (namely the sea–land thermal contrast) or to the location of Dunkerque at the entrance of the English Channel.

4.8 | Events' durations

Such an analysis is not common in the literature: for Aird *et al.* (2021), it was done relying on 6 months of high-resolution simulations using the Weather and Research Forecast model over Iowa (USA), whereas Weide Luiz and Fiedler (2022) used 3 months of Doppler lidar observations recorded in a rural area of Germany. Both studies concern continental sites; Aird *et al.* (2021) covers winter and spring, whereas Weide Luiz and Fiedler (2022) bears on the summer. The event duration distributions presented in these two studies are very similar to the one observed in Dunkerque, despite the type of site being very different: the event frequency quickly decreases with increasing jet duration, so that short events dominate the distribution. Although events lasting up to around 20 hr could be detected over the three sites, the average duration was around 3–4 hr, with about two-thirds of the events lasting less than 4 hr.

4.9 | Conditions of jet occurrence

The geostrophic wind roses obtained in Dunkerque are very similar to those reported for the Cabauw inland site by Baas *et al.* (2009). In Cabauw, as in Dunkerque, the dominant geostrophic wind direction and the strongest speeds were found from the southwest to west, and selecting only the data concurrent with the LLJs decreased the share of strong geostrophic winds and increased the share of northeasterly to southeasterly geostrophic winds. The fact that LLJs occur preferentially in weak geostrophic flows is coherent with Kalverla *et al.* (2019), who found the highest LLJ frequency in the Dunkerque area for the “undefined” weather pattern, which corresponds to the absence of well-defined synoptic forcing. The predominance of easterly geostrophic flows during jets is another finding in agreement with Kalverla *et al.* (2019), who also obtained high LLJ frequencies in the weather patterns causing southeasterly to northeasterly flows in the Dunkerque region (both cyclonic and anticyclonic). Regarding atmospheric stability and the land–sea temperature difference, northeasterly jets occurred dominantly in an unstable atmosphere and when the land was strongly warmer than the nearby sea, which is coherent with their spring/summer and diurnal character. Conversely, the offshore jets occurred dominantly in a neutral or stable atmosphere and when the sea was warmer than the land, which is coherent with their nocturnal character. However, for the northeasterly jets, the analysis of local data was not sufficient to distinguish the different possible formation mechanisms (sea breeze or wind channeling in the Dover Strait), and for the offshore jets the hodographs also suggested the existence of at least two formation mechanisms (one of them being frictional decoupling). Therefore, the analysis in terms of direction modes allowed us to highlight efficiently some of the jet properties (annual and daily cycle, shear generation, etc.), but each of these modes cannot be associated unequivocally with a single jet formation mechanism. A manual classification of the hundreds of jet events would be necessary, followed by more work with the reanalyses to identify the set of criteria able to discriminate between the different formation mechanisms.

5 | CONCLUSIONS

In order to better characterize the LLJs occurring at low altitudes (up to 200 m AMSL) in the region of Dunkerque (northern coast of France, southernmost North Sea), almost 4 years of wind profiles recorded by Doppler lidars were analyzed and the results were compared with previous observational studies concerning LLJs in the North Sea

area. Those studies presented and analyzed observations recorded over three inland and two offshore sites along the Dutch or German coast. Thus, the present work, which focuses on a coastal site located on the southern edge of the North Sea, complements those studies.

A low-altitude wind maximum was found in 11,462 of the 10-min average wind profiles, representing 5.03% of the database. For the typical LLJ occurring over Dunkerque, the altitude of the wind maximum (jet core) was located at 114 m AMSL, with a core wind speed around 7–8 m·s⁻¹. The core height distributions looked similar to what was reported for the North Sea sites located closest to Dunkerque. The core speed distribution resembled the one found at the closest inland site (Cabauw) but included fewer high-speed values. The core wind direction exhibited a dominant mode in the northeasterly direction, and a secondary mode in the eastsoutheasterly direction, the remaining cases being subdivided into a southerly and a “westerly + northwesterly” mode. As was previously reported, the strongest jets tended to be located at higher altitudes. The northeasterly jets were only observed at the closest offshore site, possibly because it is located close enough to the English Channel to be impacted by the wind channeling effect in the Dover Strait, which has been previously described in the literature. Conversely, the southwesterly jets that are very frequent at the other sites, and even dominant at the offshore sites, were almost absent in Dunkerque. This difference might be explained by the fact that the lidar in Dunkerque missed some of those southwesterly jets (due to a slightly lower maximum range compared with the other sites).

The LLJs were most frequent in spring and summer; more precisely, the month with the highest LLJ frequency, and also the largest number of strong jets, was April. In contrast, LLJs were the least frequent in February. This annual cycle was mainly related to that of the dominant northeasterly LLJ mode, which disappeared from October to February but peaked in April and remained frequent until August. On the contrary, southerly jets were dominant in the cold season, from October to January. The northeasterly onshore mode occurred mostly in the daytime, whereas the two offshore modes (eastsoutheasterly and southerly) were almost exclusively nocturnal. Consequently, there were two daily high-activity periods for the jets, in the late night (0000 to 0700 UTC) and in the afternoon (1200 to 1800 UTC), whereas the LLJ frequency dropped in the morning (0800 to 1100 UTC). The afternoon peak in LLJ frequency was not observed at any of the other sites in the North Sea area, indicating that the northeasterly mode is related to a coastal jet formation mechanism (the sea–land temperature contrast) or with a wind channeling effect in the Dover Strait. The longest jet event recorded over Dunkerque lasted more than 26 hr,

with 18% of the events that lasted from 1 to 2 hr and 46% from 2 to 18 hr.

ERA5 data were used to investigate the conditions of occurrence and possible formation mechanisms of the LLJs over Dunkerque. Two parameters were investigated: the local land–sea thermal contrast, and the geostrophic wind computed from the regional 850 hPa geopotential gradient. The Pasquill stability classes derived from the ultrasonic anemometer observations were also used to assess the atmospheric stability. The northeasterly LLJ mode mostly occurred when the air over land was warmer than over the sea, under light to moderate easterly geostrophic winds corresponding to anticyclonic continental flows; it was also preferentially associated with a slightly or plainly unstable atmosphere. Therefore, this mode likely consisted of sea breezes and jets generated by the wind channeling through the Dover Strait, though the proportion of local and regional LLJs was not investigated in the present work. The southerly mode mostly occurred when the land was colder than the sea, under a slightly or plainly stable atmosphere, and under moderate to strong southwesterly geostrophic winds, corresponding to cyclonic flows bringing oceanic air masses over Dunkerque, with possible frontal passages. The properties and conditions of occurrence of the two other LLJ modes (east-southeasterly and westerly + northwesterly) suggested the existence of at least two formation mechanisms for each mode, with the east-southeasterly mode likely including frictional decoupling/inertial oscillation, whereas the westerly + northwesterly mode likely included sea breezes.

In conclusion, this work highlighted the differences that may exist in terms of LLJs between inland, coastal, and offshore sites, even located along the same coast, due to the contribution of local coastal phenomena (sea/land breezes) and regional phenomena associated with the shape of the coast (channeling in the Dover Strait). It is now planned to study wind profiles with a higher vertical extent, in order to check what types of LLJs exist more in altitude and what their frequency is compared with the very low altitude jets. A more thorough study with the reanalysis data should also be performed to check if the model properly reproduces the LLJs' variability on a coastal site such as Dunkerque. Future work should also aim at quantifying the respective contributions of local, regional, and large-scale phenomena responsible for LLJ formation over Dunkerque and the southern North Sea, using weather reanalysis data on a larger domain and/or modeling studies. Finally, the formation mechanisms of offshore LLJ that do not correspond to frictional decoupling should be investigated using modeling studies.

AUTHOR CONTRIBUTIONS

Elsa Dieudonné: Conceptualization; formal analysis; methodology; software; writing – original draft; writing – review and editing. **Hervé Delbarre:** Conceptualization; funding acquisition; project administration; writing – review and editing. **Anton Sokolov:** Resources; writing – review and editing. **Felix Ebojje:** Methodology; writing – original draft; writing – review and editing. **Patrick Augustin:** Data curation; investigation; writing – review and editing. **Marc Fourmentin:** Data curation; investigation; writing – review and editing.

ACKNOWLEDGEMENTS

We warmly thank WPD France (Wind Power Development) for providing the Doppler lidar data for the period August 2016–July 2017 and making it available for this work. We also thank ECMWF for providing the ERA-5 data and Michael Sprenger (ETH Zurich) for his support in providing the data. Some statistical calculations and data treatment for this paper were carried out using the CALCULCO computing platform, supported by Service Commun du Système d'Information de l'Université du Littoral Côte d'Opale (ScoSI/ULCO). This study was funded by the CPER project Climibio (<http://climibio.univ-lille.fr/>); in this respect, we thank the Regional Council of Région Hauts-de-France, the Ministère de l'Enseignement Supérieur et de la Recherche and the European Regional Development Fund (ERDF) for their financial support. This project also benefited from the CaPPA project (Chemical and Physical Properties of the Atmosphere, <https://www.labex-cappa.fr/>), which is funded by the French National Research Agency (ANR) through the PIA (Programme d'Investissement d'Avenir) under the contract ANR-11-LABX-0005-01, by the Regional Council of the Région Hauts-de-France and by the ERDF.

FUNDING INFORMATION

This study was funded by the Regional Council of Région Hauts-de-France, the French Ministère de l'Enseignement Supérieur et de la Recherche, and the European Fund for Regional Economic Development (FEDER) through the CPER project Climibio. This project was also funded by the French National Research Agency (ANR) through the PIA (Programme d'Investissement d'Avenir) under the contract ANR-11-LABX-0005-01, by the Regional Council of the Région Hauts-de-France, and by the FEDER through the CaPPA project (Chemical and Physical Properties of the Atmosphere). The wind lidar data recorded prior to September 2017 were provided free of charge by WPD France in the framework of a non-profit scientific collaboration agreement between LPCA/ULCO and WPD France.

CONFLICT OF INTEREST STATEMENT

The authors have no conflict of interest to declare about this study.

DATA AVAILABILITY STATEMENT

The sonic anemometer data, along with the wind lidar data recorded from November 2017, are available from the corresponding author upon reasonable request. The wind lidar data recorded prior to September 2017 belong to WPD France (Wind Power Development) and the authors do not have permission to share them. The raw ECMWF reanalysis data are available from the Climate Data Store of the Copernicus Climate Change Service (<https://cds.climate.copernicus.eu/>). Data derived from the reanalyses are available upon request from the corresponding author.

ORCID

Elsa Dieudonné  <https://orcid.org/0000-0001-5320-243X>

Hervé Delbarre  <https://orcid.org/0000-0001-8596-9467>

Anton Sokolov  <https://orcid.org/0000-0001-9236-5864>

Patrick Augustin  <https://orcid.org/0000-0003-0966-2468>

Marc Fourmentin  <https://orcid.org/0000-0003-1385-2547>

REFERENCES

- Aird, J.A., Barthelmie, R.J., Shepherd, T.J. and Pryor, S.C. (2022) Occurrence of low-level jets over the eastern U.S. coastal zone at heights relevant to wind energy. *Energies*, 15, 445. <https://doi.org/10.3390/en15020445>.
- Aird, J.A., Barthelmie, R.J., Shepherd, T.J. and Pryor, S.C. (2021) WRF-simulated low-level jets over Iowa: characterization and sensitivity studies. *Wind Energy Science*, 6, 1015–1030. <https://doi.org/10.5194/wes-6-1015-2021>.
- Andreas, E.L., Claffy, K.J. and Makshatas, A.P. (2000) Low-level atmospheric jets and inversions over the Western Weddell Sea. *Boundary-Layer Meteorology*, 97, 459–486. <https://doi.org/10.1023/A:1002793831076>.
- Arritt, R.W., Rink, T.D., Segal, M., Todey, D.P., Clark, C.A., Mitchell, M.J. and Labas, K.M. (1997) The Great Plains low-level jet during the warm season of 1993. *Monthly Weather Review*, 125, 2176–2192. [https://doi.org/10.1175/1520-0493\(1997\)125<2176:TGPLLJ>2.0.CO;2](https://doi.org/10.1175/1520-0493(1997)125<2176:TGPLLJ>2.0.CO;2).
- Baas, P., Bosveld, F.C., Baltink, H.K. and Holtslag, A.M. (2009) A climatology of nocturnal low-level jets at Cabauw. *Journal of Applied Meteorology and Climatology*, 48, 1627–1642. <https://doi.org/10.1175/2009JAMC1965.1>.
- Banta, R.M., Newsom, R.K., Lundquist, J.K., Pichugina, Y.L., Coulter, R.L. and Mahrt, L. (2002) Nocturnal low-level jet characteristics over Kansas during Cases-99. *Boundary-Layer Meteorology*, 105, 221–252. <https://doi.org/10.1023/A:1019992330866>.
- Banta, R.M., Pichugina, Y.L. and Brewer, W.A. (2006) Turbulent velocity-variance profiles in the stable boundary layer generated by a nocturnal low-level jet. *Journal of the Atmospheric Sciences*, 63, 2700–2719. <https://doi.org/10.1175/JAS3776.1>.
- Banta, R.M., Senff, C.J., White, A.B., Trainer, M., McNider, R.T., Valente, R.J., Mayor, S.D., Alvarez, R.J., Hardesty, R.M., Parrish, D. and Fehsenfeld, F.C. (1998) Daytime buildup and nighttime transport of urban ozone in the boundary layer during a stagnation episode. *Journal of Geophysical Research: Atmospheres*, 103, 22519–22544. <https://doi.org/10.1029/98JD01020>.
- Bardal, L.M., Onstad, A.E., Sætran, L.R. and Lund, J.A. (2018) Evaluation of methods for estimating atmospheric stability at two coastal sites. *Wind Engineering*, 42, 561–575.
- Blackadar, A.K. (1957) Boundary layer wind maxima and their significance for the growth of nocturnal inversions. *Bulletin of the American Meteorological Society*, 38, 283–290. <https://doi.org/10.1175/1520-0477-38.5.283>.
- Bonner, W.D. (1968) Climatology of the low-level jet. *Monthly Weather Review*, 96, 833–850. [https://doi.org/10.1175/1520-0493\(1968\)096<0833:COTLLJ>2.0.CO;2](https://doi.org/10.1175/1520-0493(1968)096<0833:COTLLJ>2.0.CO;2).
- Capon, R.A. (2003) Wind speed-up in the Dover Straits with the met Office new dynamics model. *Meteorological Applications*, 10, 229–237. <https://doi.org/10.1017/S1350482703003037>.
- Christakos, K., Varlas, G., Reuder, J., Kastafados, P. and Papadopoulos, A. (2014) Analysis of a low-level coastal jet off the Western coast of Norway. *Energy Procedia*, 53, 162–172. <https://doi.org/10.1016/j.egypro.2014.07.225>.
- Corsmeier, U. (1997) Ozone concentration jump in the stable nocturnal boundary layer during a LLJ-event. *Atmospheric Environment*, 31, 1977–1989. [https://doi.org/10.1016/S1352-2310\(96\)00358-5](https://doi.org/10.1016/S1352-2310(96)00358-5).
- Du, Y., Zhang, Q., Ying, Y. and Yang, Y. (2012) Characteristics of low-level jets in Shanghai during the 2008–2009 warm seasons as inferred from wind profiler radar data. *Journal of the Meteorological Society of Japan*, 90, 891–903. <https://doi.org/10.2151/jmsj.2012-603>.
- Duncan, J.B. (2018) Observational analyses of the North Sea low-level jet (TNO report No. TNO 2018 R11428). Technical University Delft (NL).
- FAA Safety Team. (2008) Wind shear (No. FAA-P-8740-40 / HQ101130). Federal Aviation Administration (FAA).
- Farquharson, J.S. (1939) The diurnal variation of wind over tropical Africa. *Quarterly Journal of the Royal Meteorological Society*, 65, 165–184. <https://doi.org/10.1002/qj.49706528004>.
- Frisch, A.S., Orr, B.W. and Martner, B.E. (1992) Doppler radar observations of the development of a boundary-layer nocturnal jet. *Monthly Weather Review*, 120, 3–16. [https://doi.org/10.1175/1520-0493\(1992\)120<0003:DROOTD>2.0.CO;2](https://doi.org/10.1175/1520-0493(1992)120<0003:DROOTD>2.0.CO;2).
- Golder, D. (1972) Relations among stability parameters in the surface layer. *Boundary-Layer Meteorology*, 3, 47–58. <https://doi.org/10.1007/BF00769106>.
- Golding, W. (2005) Low-level Windshear and its impact on airlines. *Journal of Aviation/Aerospace Education & Research*, 14. <https://doi.org/10.15394/jaaer.2005.1530>.
- Gouault, J. (1938) Vents en altitude a fort Lamy (Tchad). *Ann. Phys. Globe France d'Outremer*, 5, 70–72 82–91.
- Gutierrez, W., Araya, G., Basu, S., Ruiz-Columbie, A. and Castillo, L. (2014) Toward understanding low level jet climatology over West Texas and its impact on wind energy. *Journal of Physics Conference Series*, 524, 012008. <https://doi.org/10.1088/1742-6596/524/1/012008>.
- Hallgren, C., Arnqvist, J., Nilsson, E., Ivanell, S., Shapkalijevski, M., Thomasson, A., Pettersson, H. and Sahlée, E. (2022) Classification and properties of non-idealized coastal wind profiles – an

- observational study. *Wind Energy Science*, 7, 1183–1207. <https://doi.org/10.5194/wes-7-1183-2022>.
- Hersbach, H., Bell, B., Berrisford, P., Hirahara, S., Horányi, A., Muñoz-Sabater, J., Nicolas, J., Peubey, C., Radu, R., Schepers, D., Simmons, A., Soci, C., Abdalla, S., Abellan, X., Balsamo, G., Bechtold, P., Biavati, G., Bidlot, J., Bonavita, M., Chiara, G.D., Dahlgren, P., Dee, D., Diamantakis, M., Dragani, R., Flemming, J., Forbes, R., Fuentes, M., Geer, A., Haimberger, L., Healy, S., Hogan, R.J., Hólm, E., Janisková, M., Keeley, S., Laloyaux, P., Lopez, P., Lupu, C., Radnoti, G., Rosnay, P.d., Rozum, I., Vamborg, F., Villaume, S. and Thépaut, J.-N. (2020) The ERA5 global reanalysis. *Quarterly Journal of the Royal Meteorological Society*, 146, 1999–2049. <https://doi.org/10.1002/qj.3803>.
- Kalverla, P.C., Duncan, J.B., Jr., Steeneveld, G.-J. and Holtlag, A.A.M. (2019) Low-level jets over the North Sea based on ERA5 and observations: together they do better. *Wind Energy Science*, 4, 193–209. <https://doi.org/10.5194/wes-4-193-2019>.
- Kalverla, P.C., Steeneveld, G.-J., Ronda, R.J. and Holtlag, A.A.M. (2017) An observational climatology of anomalous wind events at offshore meteorological masts (North Sea). *Journal of Wind Engineering and Industrial Aerodynamics*, 165, 86–99. <https://doi.org/10.1016/j.jweia.2017.03.008>.
- Karipot, A., Leclerc, M.Y., Zhang, G., Martin, T., Starr, G., Hollinger, D., McCaughey, J.H. and Hendrey, G.R. (2006) Nocturnal CO₂ exchange over a tall forest canopy associated with intermittent low-level jet activity. *Theoretical and Applied Climatology*, 85, 243–248. <https://doi.org/10.1007/s00704-005-0183-7>.
- Kettle, A.J. (2014) Unexpected vertical wind speed profiles in the boundary layer over the southern North Sea. *Journal of Wind Engineering and Industrial Aerodynamics*, 134, 149–162. <https://doi.org/10.1016/j.jweia.2014.07.012>.
- Klein, A., Ravetta, F., Thomas, J.L., Ancellet, G., Augustin, P., Wilson, R., Dieudonné, E., Fourmentin, M., Delbarre, H. and Pelon, J. (2019) Influence of vertical mixing and nighttime transport on surface ozone variability in the morning in Paris and the surrounding region. *Atmospheric Environment*, 197, 92–102. <https://doi.org/10.1016/j.atmosenv.2018.10.009>.
- Maddox, R.A. (1983) Large-scale meteorological conditions associated with midlatitude mesoscale convective complexes. *Monthly Weather Review*, 111, 1475–1493. [https://doi.org/10.1175/1520-0493\(1983\)111<1475:LSMCAW>2.0.CO;2](https://doi.org/10.1175/1520-0493(1983)111<1475:LSMCAW>2.0.CO;2).
- Mahrt, L. (1999) Stratified atmospheric boundary layers. *Boundary-Layer Meteorology*, 90, 375–396. <https://doi.org/10.1023/A:1001765727956>.
- Mathieu, N., Strachan, I.B., Leclerc, M.Y., Karipot, A. and Pattey, E. (2005) Role of low-level jets and boundary-layer properties on the NBL budget technique. *Agricultural and Forest Meteorology*, 135, 35–43. <https://doi.org/10.1016/j.agrformet.2005.10.001>.
- McCorcle, M.D. (1988) Simulation of surface-moisture effects on the Great Plains low-level jet. *Monthly Weather Review*, 116, 1705–1720. [https://doi.org/10.1175/1520-0493\(1988\)116<1705:SOSMEO>2.0.CO;2](https://doi.org/10.1175/1520-0493(1988)116<1705:SOSMEO>2.0.CO;2).
- Means, L.L. (1952) On thunderstorm forecasting in the Central United States. *Monthly Weather Review*, 80, 165–189. [https://doi.org/10.1175/1520-0493\(1952\)080<0165:OTFITC>2.0.CO;2](https://doi.org/10.1175/1520-0493(1952)080<0165:OTFITC>2.0.CO;2).
- Means, L.L. (1944) The nocturnal maximum occurrence of thunderstorms in the Midwestern States (No. 16), Miscellaneous reports. University of Chicago Press.
- Meeus, J.H. (1991) *Astronomical Algorithms*. Richmond: Willmann-Bell, Inc.
- Mo, K.C., Noguez-Paele, J. and Paele, J. (1995) Physical mechanisms of the 1993 summer floods. *Journal of the Atmospheric Sciences*, 52, 879–895. [https://doi.org/10.1175/1520-0469\(1995\)052<0879:PMOTSF>2.0.CO;2](https://doi.org/10.1175/1520-0469(1995)052<0879:PMOTSF>2.0.CO;2).
- Mohan, M. and Siddiqui, T.A. (1998) Analysis of various schemes for the estimation of atmospheric stability classification. *Atmospheric Environment*, 32, 3775–3781. [https://doi.org/10.1016/S1352-2310\(98\)00109-5](https://doi.org/10.1016/S1352-2310(98)00109-5).
- Møller, M., Domagalski, P. and Sætran, L.R. (2020) Comparing abnormalities in onshore and offshore vertical wind profiles. *Wind Energy Science*, 5, 391–411. <https://doi.org/10.5194/wes-5-391-2020>.
- Nunalee, C.G. and Basu, S. (2014) Mesoscale modeling of coastal low-level jets: implications for offshore wind resource estimation. *Wind Energy*, 17, 1199–1216. <https://doi.org/10.1002/we.1628>.
- Rodrigo, J.S., Cantero, E., García, B., Borbón, F., Irigoyen, U., Lozano, S., Fernand, P.M. and Chávez, R.A. (2015) Atmospheric stability assessment for the characterization of offshore wind conditions. *Journal of Physics Conference Series*, 625, 012044. <https://doi.org/10.1088/1742-6596/625/1/012044>.
- Schwerdtfeger, W. (1975) The effect of the Antarctic peninsula on the temperature regime of the Weddell Sea. *Monthly Weather Review*, 103, 45–51. [https://doi.org/10.1175/1520-0493\(1975\)103<0045:TEOTAP>2.0.CO;2](https://doi.org/10.1175/1520-0493(1975)103<0045:TEOTAP>2.0.CO;2).
- Sharples, J.J. (2009) An overview of mountain meteorological effects relevant to fire behaviour and bushfire risk. *International Journal of Wildland Fire*, 18, 737–754. <https://doi.org/10.1071/WF08041>.
- Smedman, A.-S., Bergström, H. and Högström, U. (1995) Spectra, variances and length scales in a marine stable boundary layer dominated by a low level jet. *Boundary-Layer Meteorology*, 76, 211–232. <https://doi.org/10.1007/BF00709352>.
- Smedman, A.-S., Tjernström, M. and Högström, U. (1993) Analysis of the turbulence structure of a marine low-level jet. *Boundary-Layer Meteorology*, 66, 105–126. <https://doi.org/10.1007/BF00705462>.
- Song, J., Liao, K., Coulter, R.L. and Lesht, B.M. (2005) Climatology of the low-level jet at the southern Great Plains atmospheric boundary layer experiments site. *Journal of Applied Meteorology and Climatology*, 44, 1593–1606. <https://doi.org/10.1175/JAM2294.1>.
- Wagner, D., Steinfeld, G., Witha, B., Wurps, H. and Reuder, J. (2019b) Low level jets over the southern North Sea. *Meteorologische Zeitschrift*, 28, 389–415. <https://doi.org/10.1127/metz/2019/0948>.
- Wagner, J., Gerz, T., Wildmann, N. and Gramitzky, K. (2019a) Long-term simulation of the boundary layer flow over the double-ridge site during the Perdigão 2017 field campaign. *Atmospheric Chemistry and Physics*, 19, 1129–1146. <https://doi.org/10.5194/acp-19-1129-2019>.
- Weide Luiz, E. and Fiedler, S. (2022) Spatiotemporal observations of nocturnal low-level jets and impacts on wind power production. *Wind Energy Science*, 7, 1575–1591. <https://doi.org/10.5194/wes-7-1575-2022>.
- Whiteman, C.D., Bian, X. and Zhong, S. (1997) Low-level jet climatology from enhanced Rawinsonde observations at a site in the southern Great Plains. *Journal of Applied Meteorology and Climatology*, 36, 1363–1376. [https://doi.org/10.1175/1520-0450\(1997\)036<1363:LLJCFE>2.0.CO;2](https://doi.org/10.1175/1520-0450(1997)036<1363:LLJCFE>2.0.CO;2).
- Wildmann, N., Hagen, M. and Gerz, T. (2022) Enhanced resource assessment and atmospheric monitoring of the research wind

- farm WiValdi. *Journal of Physics Conference Series*, 2265, 022029. <https://doi.org/10.1088/1742-6596/2265/2/022029>.
- Wu, Y. and Raman, S. (1998) The summertime Great Plains low level jet and the effect of its origin on moisture transport. *Boundary-Layer Meteorology*, 88, 445–466. <https://doi.org/10.1023/A:1001518302649>.
- Xiang, Y. (2011) *Analyse dynamique en champ proche de la contribution des sources de composés organiques volatils, en région urbaine sous influence industrielle* (PhD thesis). Université du Littoral Côte d'Opale. <http://www.theses.fr/2011DUNK0408>.
- Zhong, S., Fast, J.D. and Bian, X. (1996) A case study of the Great Plains low-level jet using wind profiler network data and a high-resolution mesoscale model. *Monthly Weather Review*, 124, 785–806. [https://doi.org/10.1175/1520-0493\(1996\)124<0785:ACSOTG>2.0.CO;2](https://doi.org/10.1175/1520-0493(1996)124<0785:ACSOTG>2.0.CO;2).
- Ziemann, A., Galvez Arboleda, A. and Lampert, A. (2020) Comparison of wind Lidar data and numerical simulations of the low-level jet at a grassland site. *Energies*, 13, 6264. <https://doi.org/10.3390/en13236264>.

SUPPORTING INFORMATION

Additional supporting information can be found online in the Supporting Information section at the end of this article.

How to cite this article: Dieudonné, E., Delbarre, H., Sokolov, A., Ebojie, F., Augustin, P. & Fourmentin, M. (2023) Characteristics of the low-level jets observed over Dunkerque (North Sea French coast) using 4 years of wind lidar data. *Quarterly Journal of the Royal Meteorological Society*, 149(754), 1745–1768. Available from: <https://doi.org/10.1002/qj.4480>